



Cite this: *J. Mater. Chem. C*, 2022, 10, 13499

## Multiple-boron–nitrogen (multi-BN) doped $\pi$ -conjugated systems for optoelectronics

Xiaobin Chen,<sup>†</sup> Dehui Tan<sup>†</sup> and Deng-Tao Yang \*

Boron–nitrogen-doped  $\pi$ -conjugated systems have been regarded as a class of organic materials with exceptional electronic and optical properties, which makes them promising in optoelectronic devices. Due to the isoelectronic relationship between the carbon–carbon (CC) unit and the boron–nitrogen (BN) unit, the location, number and orientation of BN units in  $\pi$ -conjugated systems bearing more than one BN unit are believed to have significant impacts on their electronic properties and intermolecular interactions. In addition, the coordination pattern of boron atoms in the conjugated systems could drastically tune their optoelectronic properties. This structural uniqueness makes these multiple-boron–nitrogen (multi-BN) doped  $\pi$ -conjugated systems exhibit great potential for application in organic light emitting diodes (OLEDs), organic photovoltaics (OPVs), and organic field-effect transistors (OFETs). This review covers recent advances in multiple boron–nitrogen doped  $\pi$ -conjugated systems including their synthetic strategies and applications in optoelectronic devices. We will rationalize the relationship between optoelectronic properties and the location, number and orientation of BN dopants as well as the coordination number of boron atoms, which could enlighten the design and synthesis of multi-BN-doped optoelectronic materials with better performances.

Received 18th March 2022,  
Accepted 10th May 2022

DOI: 10.1039/d2tc01106a

rsc.li/materials-c

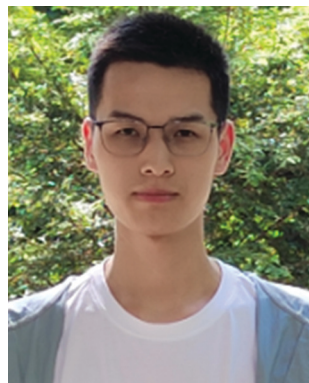
### 1. Introduction

Tunable properties and flexibility have made organic  $\pi$ -conjugated systems attractive targets for applications in organic light emitting diodes (OLEDs),<sup>1,2</sup> organic photovoltaics (OPVs),<sup>3,4</sup> and organic field-effect transistors (OFETs).<sup>5–7</sup> Besides optimizing the optoelectronic device structures, searching for new organic molecules

with advanced performance is also the other aspect of pursuing higher performances of devices. The optoelectronic properties of organic molecules often can be significantly altered by subtle changes in their molecular structures.<sup>8–10</sup> Doping heteroatoms into organic  $\pi$ -conjugated molecules has attracted increasing attention because it not only can increase the structural diversity of the parent organic  $\pi$ -conjugated systems, but can also endow them with novel physical and chemical properties.<sup>11,12</sup> Boron as a dopant has received exceptional attention due to its empty  $p_z$  orbital; however, the instability of boron-doped organic molecules usually limits their practical applications as organic functional materials.<sup>13,14</sup> In addition to increasing the stability of boron-

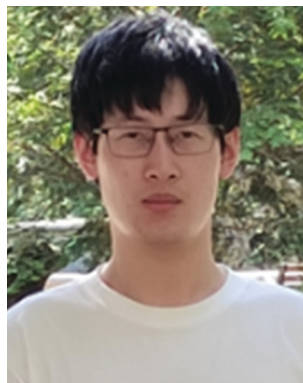
*School of Chemistry and Chemical Engineering, Northwestern Polytechnical University, Xi'an, Shaanxi 710072, China. E-mail: dtyang@nwpu.edu.cn*

<sup>†</sup> X. C. and D. T. contributed equally to this work. First authorship was determined by coin toss.



Xiaobin Chen

Xiaobin Chen received his bachelor's degree from the School of Materials Science and Engineering, Luoyang Institute of Science and Technology, in 2020. He is currently pursuing his master's degree at the School of Chemistry and Chemical Engineering, Northwestern Polytechnical University, under the supervision of Prof. Deng-Tao Yang. His research interest is in MR-TADF materials.



Dehui Tan

Dehui Tan received his bachelor's degree from the School of Chemistry and Chemical Engineering, Hefei University of Technology, in 2020. He is currently studying for his master's degree at the School of Chemistry and Chemical Engineering, Northwestern Polytechnical University, under the supervision of Prof. Deng-Tao Yang. His research interest is in the synthesis of boron-based chiral CPL molecules.

doped molecules by either introducing bulky substituents on boron atoms or doping boron into constraint structures, replacing the carbon-carbon (CC) unit in organic  $\pi$ -conjugated molecules with the isoelectronic counterpart-boron-nitrogen (BN) unit has been shown to be an effective strategy to improve their stability.<sup>15</sup> The introduction of the BN unit can produce novel organic optoelectronic materials with similar structures to their all-carbon analogues but distinct electronic and optical properties due to the dipolar nature of the BN unit.<sup>16-19</sup> In the past decades, plenty of BN-doped polycyclic arenes have been reported, and their applications have been applied in various areas.<sup>18,19</sup> BN-doped polycyclic aromatic hydrocarbons (PAHs) have been found to exhibit better charge transport performance in OFETs with better stability.<sup>20-22</sup> Discrete boron and nitrogen atoms in PAHs can induce multi-resonant HOMO-LUMO separation, giving rising to thermally activated delayed fluorescence (TADF) with narrow-band emission.<sup>23</sup> Organoboron compounds doped with the BN unit with tetracoordinated boron atoms display excellent electron-injecting and -transporting properties because of their rather low LUMO energy levels.<sup>24-26</sup>

From a molecular engineering point of view, the number, location, and orientation of BN units could adjust the overall dipolar nature of BN-doped molecules, resulting in distinct electronic and optical properties. For example, BN-doped PAHs with different BN locations could display entirely different optoelectronic properties.<sup>27-32</sup> In addition, the unique coordination pattern of boron atoms could further enrich the structural diversity of BN-doped molecules. Mono-BN-doped organic  $\pi$ -conjugated systems have been recently summarized by several reviews.<sup>16-19,33-36</sup> However, although there are increasing reports on multi-BN-doped organic  $\pi$ -conjugated molecules, a review summarizing how to utilize different doping patterns (different numbers, locations and orientations of multiple BN units) to design multi-BN-doped organic  $\pi$ -conjugated molecules and how the doping pattern affects their properties and applications is still highly desired. In this review, we focus on molecular structures bearing two and more BN units and

rationalize the relationship between optoelectronic properties and BN units' doping patterns. Of course, we will also pay attention to their synthetic methodologies since they are still the bottle-neck for constructing the designed structures, which limits the applications of BN-doped molecules in optoelectronics. In order to systematically investigate the effect of BN-dopants on properties, we will compare the differences of electronic and optical properties if the same PAHs with multiple BN units have more than one BN-doped analogue; otherwise, we will compare multi-BN-doped molecules with either mono-BN-doped versions or all-carbon analogues depending on their availability. The review will be divided into three sections. Firstly, we will summarize multi-BN-doped  $\pi$ -conjugated systems with bonded boron and nitrogen atoms, which have been widely used in various areas including OFETs. Secondly, multi-BN-doped  $\pi$ -conjugated systems with discrete boron and nitrogen atoms will be discussed, and 1,4-BN-doped PAHs with multi-resonant HOMO-LUMO separation effects will be the focus of attention. Thirdly, we will discuss multi-BN-doped  $\pi$ -conjugated systems bearing tetracoordinate boron atoms, which usually have low LUMOs and could be used in charge transport devices. The molecules with one BN unit will only be discussed when needed to compare with their multi-BN doped analogues. BN-doped polymers for optoelectronics are out of scope of this review.

## 2. Multi-BN-doped $\pi$ -conjugated systems with bonded boron and nitrogen atoms

BN-doped benzenes with bonded boron and nitrogen atoms are also named 1,2-azaborines. In order to distinguish different BN-doped locations in PAHs, we simply divide them into three categories (Fig. 1): BN center-doped PAHs, in which the BN unit is in the center of PAHs; BN edge-doped PAHs, in which the BN unit is at the edge of PAHs; and BN partially-edge-doped PAHs, in which either the boron atom or the nitrogen atom is located at the edge of PAHs.

### 2.1 BN-PAHs

As one of the representative PAHs with three fused phenyl rings, phenanthrene **1** doped with the BN unit has been widely studied,<sup>37-41</sup> especially mono-BN-doped phenanthrenes (**2-7**) (Fig. 2).<sup>42-50</sup> However, multi-BN-doped phenanthrenes have been excluded until recently. The di-BN edge-doped phenanthrene **8** was obtained through two-fold Stille cross coupling followed by borylative cyclization (Fig. 2).<sup>51</sup> Compared to its mono-BN-doped analogue **7**, compound **8** showed a blue-shifted absorption spectrum and a red-shifted emission spectrum, resulting in a larger Stokes shift. The polarity of solvents had a negligible impact on its absorption and emission. The number of BN units has been found to have a critical impact on the bromination reaction for further functionalization.

Embedding multiple BN units into anthracene **9** has gained more attention than its isomer phenanthrene. There are different isomers of the bis-BN-doped anthracene (**10-12**),<sup>52-54</sup> as



**Deng-Tao Yang**

*Deng-Tao Yang has been a professor in the School of Chemistry and Chemical Engineering at North-western Polytechnical University since September 2020. He received his BS in Chemistry and BEng in Computer Science from Lanzhou University in 2010. After he obtained MS in Organic Chemistry from the same university in 2013, he moved to Canada and joined Prof. Suning Wang group at Queen's University pursuing his PhD degree (2013-2017). He continued his academic career at MIT as a postdoc associate (advisor: Karthish Manthiram) from 2018 to 2020. His current research interests focus on boron-based organic functional materials.*

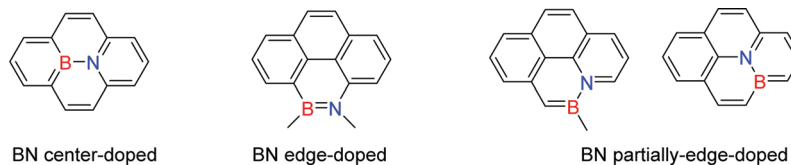


Fig. 1 The terminology of different locations of the BN unit in this review.

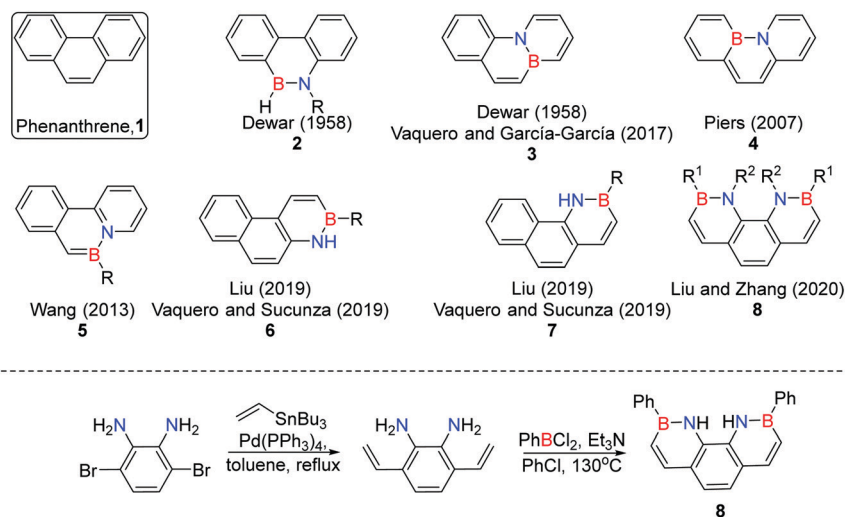


Fig. 2 Phenanthrene and BN-doped phenanthrenes and the synthesis of **8**.

shown in Fig. 3. Compounds **10** and **11** were synthesized through a double borylative cyclization reaction (Fig. 3a). A gold-catalyzed cyclization of the diamino-functionalized precursor **12a** was exploited to generate compound **12** (Fig. 3b).<sup>54</sup> Due to the lack of the photophysical properties of **10**, we will only discuss the photophysical properties of **11** and **12**. Compared to anthracene **9**, both the mono-BN-doped anthracene and **11** showed a strong second electronic transition. With respect to the emission, **11** had an almost doubled quantum yield compared with **9** and the mono-BN-doped anthracene. The well-known cycloaddition chemistry of **9** did not happen to the mono-BN-doped anthracene and **11**. In addition to the fact that compound **12** exhibited  $\sim 0.2$  eV higher HOMO and LUMO energy levels, it had quite similar absorption, emission and quantum yields to its mono-BN doped analogue, which indicates that the number of BN units does not affect the photophysical properties in this specific doping pattern. Compared to **11** that has the same number of BN units but different doping patterns, both the absorption and emission of **12** showed obvious red-shift, which indicates that the doping pattern of **12** enables better conjugation of BN units in the anthracene.

Very recently, exploiting **11** as the core structure, Wang and coworkers synthesized tetraphenyl bis-BN-doped anthracene **11-TP** and diphenyl bis-BN-doped anthracene **11-DP** from a perspective of molecular engineering (Fig. 3c).<sup>55</sup> The substituents on the boron atoms were found to have a significant impact on the charge transport properties. The unique herringbone packing mode of **11-DP** resulted in anisotropic charge transport with the

highest hole mobility of up to  $1.3 \text{ cm}^2 \text{ V}^{-1} \text{ s}^{-1}$  in OFETs. In addition, organic phototransistors (OPTs) based on **11-DP** single crystals exhibited excellent photodetector performance. In addition to constructing brand-new molecules, this work points out another direction to discover optoelectronic molecules with excellent performance.

Attention has been paid to BN-pyrenes due to their rigid conjugated structures and high fluorescence.<sup>52,56–58</sup> In addition to mono-BN-doped pyrenes, bis-BN-doped pyrenes have also been synthesized. Dewar and coworkers reported the synthesis of bis-BN-pyrene **14** while they discovered the synthesis of bis-BN-doped anthracene **10** using double borylative cyclization (Fig. 4).<sup>52</sup> Similar to **10**, the photophysical properties of **14** have not been reported. Wang and coworkers exploited the photoelimination reaction they developed earlier to achieve the synthesis of another bis-BN-doped pyrene, **15**.<sup>59</sup> This photoelimination would be applied to construct more diverse BN-PAHs if the problem of low reaction quantum yields could be tackled, since these BN-PAHs are hardly accessed through other borylation reactions. Compared to **14**, compound **15** had a much smaller HOMO–LUMO energy gap with an increased HOMO level and a decreased LUMO level. Compared to BN-phenanthrene **5** (Fig. 2), the maxima of the absorption and fluorescence of **15** were red-shifted by  $\sim 70$  nm. Due to the instability of **15**, Wang *et al.* proposed the *in situ* exciton-driven elimination (EDE) strategy, in which the stable precursor compound **15a** was fabricated into an OLED device rather than the unstable **15** and then the double elimination was driven by

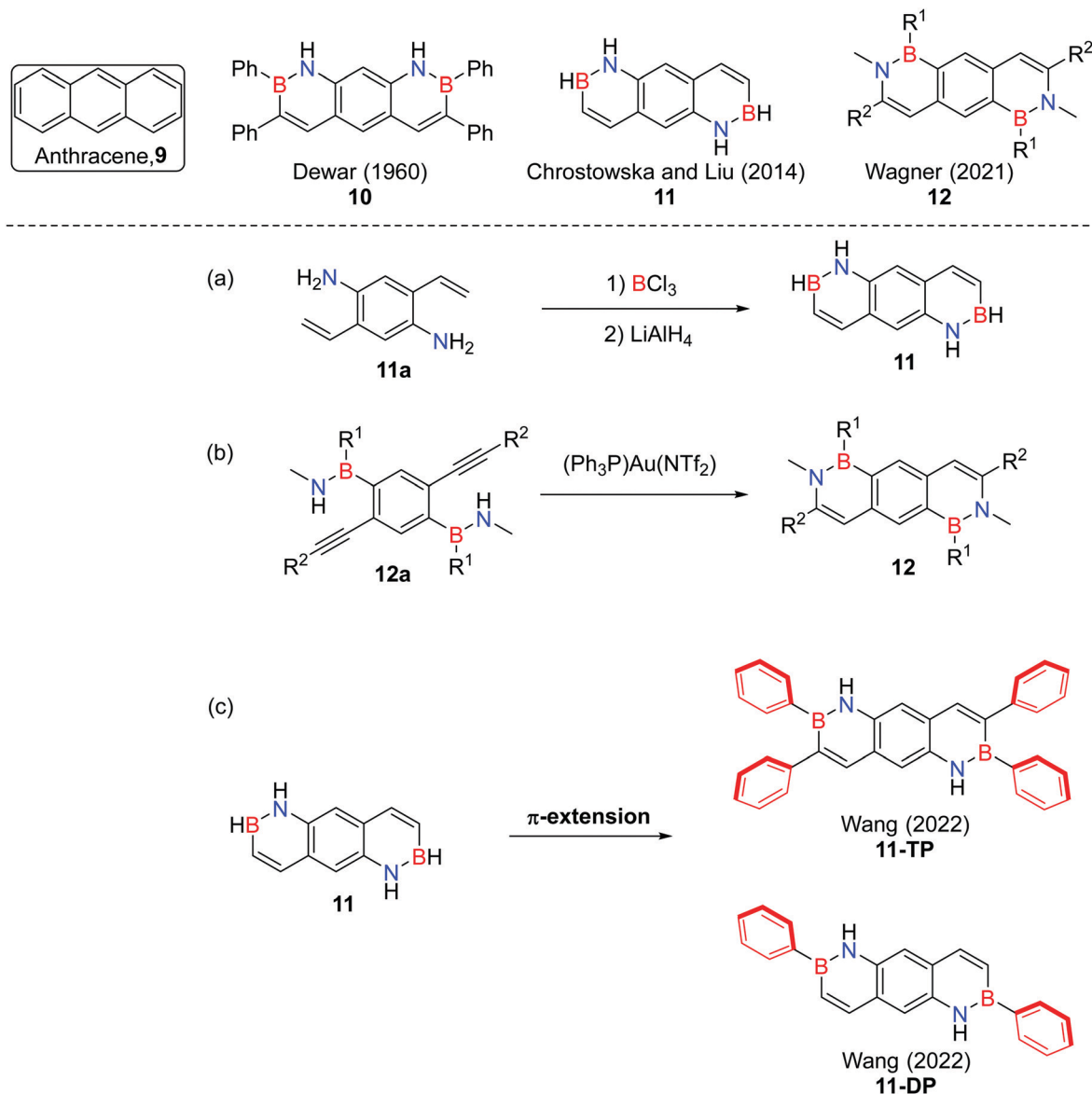


Fig. 3 Examples of bis-BN-doped anthracenes.

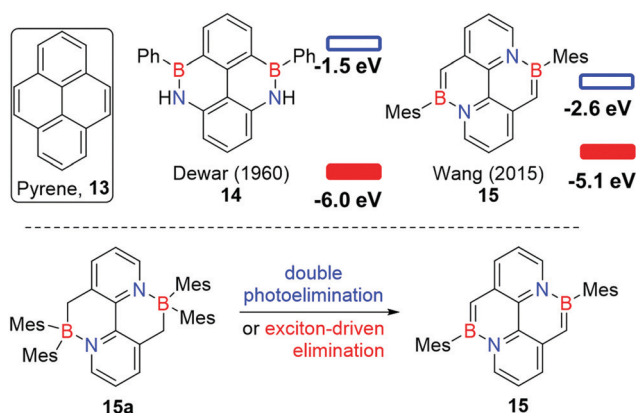


Fig. 4 Bis-BN-doped pyrenes.

excitons to *in situ* generate the fluorescent bis-BN-doped 15 in the OLED device. Other BN-heterocycle precursors could also undergo EDE to generate the corresponding fully conjugated BN-arenes.

Isoelectronic to pyrene, ullazines are of great interest in dye-sensitized solar cells (DSCs).<sup>60–63</sup> Doping the BN unit into ullazines still lacks investigation; only one kind of bis-BN-doped ullazine 17 has been reported (Fig. 5).<sup>64</sup> Three different electrophilic borylation approaches have been developed to introduce a variety of functional groups on boron atoms. The HOMO energy level was significantly lowered to  $-5.78$  eV after two BN units were doped into ullazines, which is in agreement with the higher stability of 17 toward air and moisture. The fact that the doped BN units could not conjugate well with the other part of the molecule results in a larger HOMO–LUMO energy gap and less aromaticity of BN-rings. The absorption and

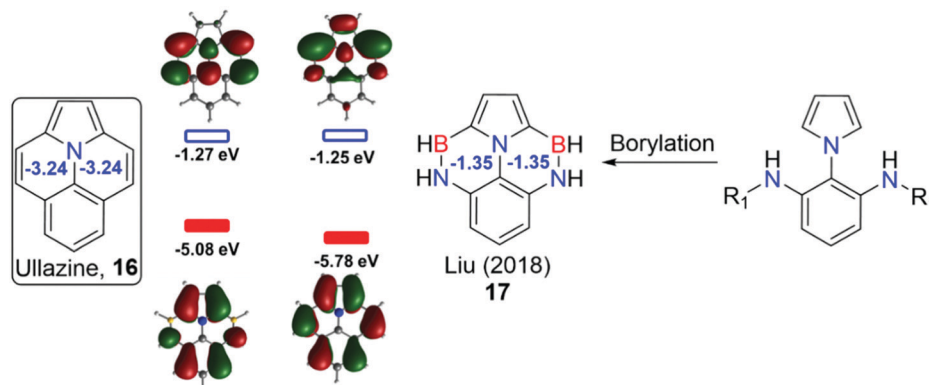


Fig. 5 Synthesis of bis-BN-doped ullazine and the numbers in blue represent the NICS.

emission spectra of bis-BN-doped ullazine **17** showed hypsochromic shift relative to the corresponding all-carbon ullazine analogues. The larger Nucleus-Independent Chemical Shifts (NICS) of **17** indicate that bis-BN-doped ullazine **17** is less aromatic than ullazine **16**.

Perylene derivatives are attractive segments of organic optoelectronic molecules. Recently, the BN unit doping patterns of perylene have been systematically investigated by the Wagner group and the Wang group (Fig. 6).<sup>32,65</sup> For the synthesis of the four bis-BN-doped perylenes **19–22**, Wagner and coworkers once again used a gold-catalyzed cyclization

reaction to generate **19** (Fig. 6a),<sup>65</sup> and Wang and coworkers developed an impressive approach to produce three bis-BN-perylenes

**20–22** using BN-naphthalene as the building block (Fig. 6b).<sup>32</sup> Compared to the parent perylene **18**, bis-BN-peryene **19** had a much larger HOMO–LUMO energy gap with an increased LUMO level and a decreased HOMO level; however, molecules **20** and **21** had similar HOMO levels, LUMO levels and HOMO–LUMO energy gaps to **18**, while **22** had a slightly smaller HOMO–LUMO energy gap with a similar HOMO level and a decreased LUMO level. The emission wavelength of **19** was

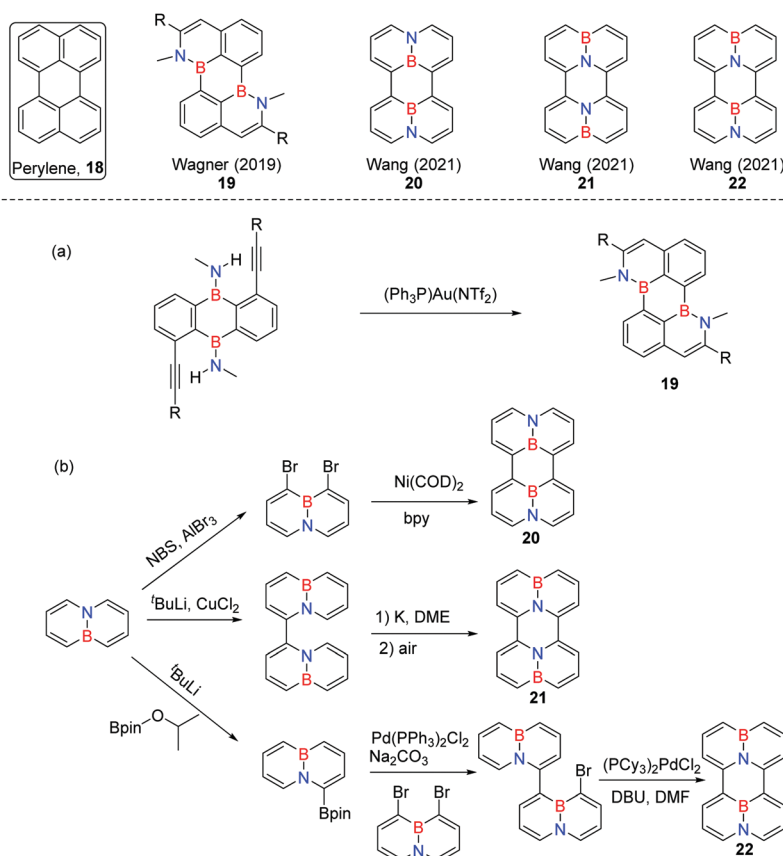


Fig. 6 Bis-BN-doped perylenes.

quite close to that of **18**, while molecules **20–22** exhibited much longer emission wavelengths than **18**. The quantum yields of all these four bis-BN-doped perylenes were much lower than that of perylene. Doping BN units into perylene did not obviously change the aromaticity of bis-BN-doped perylenes. This is a good example showing that different BN orientations of BN-perylenes could impact the solid-state packing mode, aromaticity and photophysical properties.

The other reason why perylene derivatives have been extensively studied is that they can be extended to a new ubiquitous class of molecules – perylene diimides (PDIs) which have high

chemical stability with high electron affinities and are regarded as one of the best n-type classes of semiconductors.<sup>66–70</sup> Wang and coworkers continued using BN-naphthalene as the building block and exploiting a similar strategy which was used in the synthesis of bis-BN-doped perylenes to construct bis-BN-doped PDIs **24** (Fig. 7).<sup>71</sup> (BN)<sub>2</sub>-PDIs **24** displayed similar quartet but hypsochromically shifted (about 20 nm) absorption in the range of 400–500 nm. Similar to BN-perylenes, the strong absorption of **24** was observed in the 300–375 nm window, which did not appear in the absorption of PDI **23**. Compared to the green emission of **23**, the emission of (BN)<sub>2</sub>-PDIs **24** was also green but

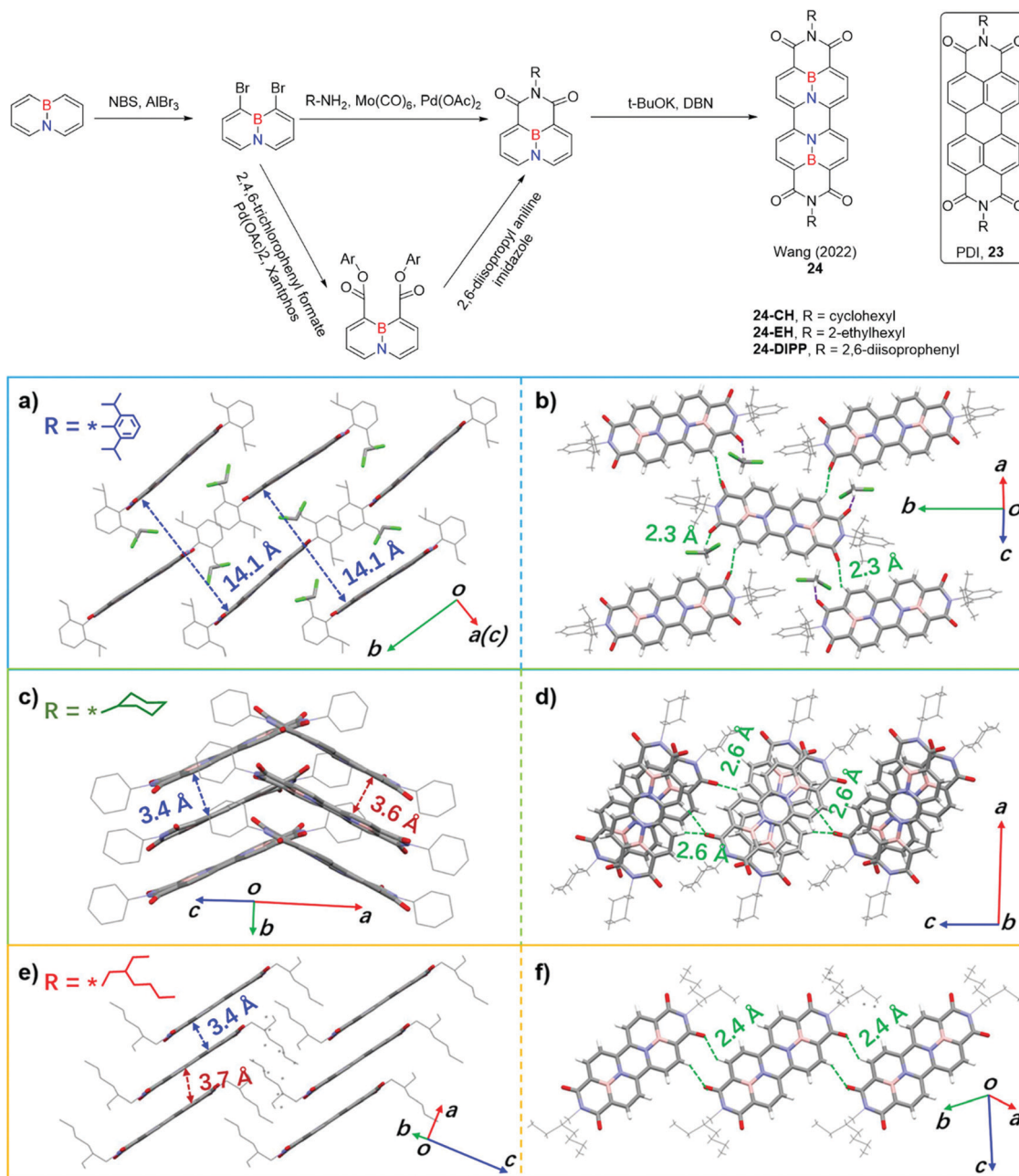


Fig. 7 Synthesis of (BN)<sub>2</sub>-PDIs, and crystal structures and packing motifs of **24-DIPP** (a and b), **24-CH** (c and d), and **24-EH** (e and f). Crystal structures of (a–f) reprinted with permission from ref. 71. Copyright 2022 American Chemical Society.

blue-shifted about 20 nm. Relative to BN-perylenes, the quantum yield of **24** was significantly decreased compared to PDI **23**. Embedding BN units into PDI could further result in a lower LUMO level. The substituents on nitrogen atoms had a significant impact on the solid-state packing modes (Fig. 7a–f). The hydrogen bonding between the C=O and hydrogen atoms of the neighboring molecules existed in the crystal structures of **24** with different substituents. The bulkiness of 2,6-diisopropylphenyl groups made 24-DIPP hardly form effective  $\pi$ - $\pi$  packing, while the less bulky functional groups in **24-CH** and **24-EH** led to cofacial packing and slipped-cofacial packing, respectively. Due to the preferred condensed crystal packing, (BN)<sub>2</sub>-PDIs **24** with 2-ethylhexyl groups on nitrogen atoms showed the highest electron mobilities up to  $0.35 \text{ cm}^2 \text{ V}^{-1} \text{ s}^{-1}$ . This once again indicates that introduction of BN units into popular organic semiconducting molecules is an effective strategy to enrich the scope of semiconducting materials.

Corannulene derivatives are an attractive class of bowl molecules in a variety of applications.<sup>72–85</sup> The synthesis of no matter the carbonaceous corannulene itself or heteroatom-doped corannulene derivatives is quite challenging. Hatakeyama *et al.* reported an efficient four-step synthesis of (BN)<sub>2</sub>-embedded corannulene **26** from commercially available starting material 4,7-dibromobenzo[c][1,2,5]thiadiazole.<sup>86</sup> Compound **26** was obtained on a multigram scale in 25% total yield of four steps, which is beneficial to providing enough material for optoelectronic applications. According to the single crystal X-ray diffraction analysis, the bowl depth of **26** was 0.15 Å (Fig. 8), which was smaller than that of corannulene (0.87 Å). NICS(0) calculations showed that the aromaticity of the five-membered ring in the center of corannulene switched from antiaromatic (8.6) to non-aromatic (−2.3) after BN units were doped. The HOMO–LUMO energy gap of **26** was smaller than that of corannulene **25** accompanied by an increased HOMO level. The higher oscillator strength (0.1762) was attributed to asymmetrization by tetrabenzo-

annulation and polarization parallel to the molecular plane induced by the two BN units. Due to the introduction of BN units, (BN)<sub>2</sub>-corannulene **26** displayed strong blue fluorescence at  $\lambda_{\text{max}} = 424 \text{ nm}$  with a quantum yield of 69%, which is almost ten times higher than that of corannulene. The first OLED based on the BN-corannulene **26** was fabricated with an external quantum efficiency of 2.61% at  $1000 \text{ cd m}^{-2}$ . The wavelength of the electroluminescence of **26** indicated a notable red-shift from 424 nm to 467 nm, which was probably caused by the  $\pi$ - $\pi$  interaction with the host material and optical interference in the OLED device.

Coronene is also known as superbenzene, which contains seven peri-fused benzene rings, and an appealing building block of organic optoelectronic materials.<sup>87</sup> Multiple-BN unit-doped coronene and its derivatives have been paid more and more attention. Very recently, Liu, Yu and coworkers reported the synthesis of bis-BN-doped coronene **28** with two syn-parallel BN units using a double BBr<sub>3</sub>-induced Scholl reaction.<sup>88</sup> The symmetry changed from  $D_{6h}$  for coronene to  $m_v$  for BN-coronene **28** (Fig. 9a). Based on the single crystal X-ray diffraction analysis, **28** adopted a slightly distorted saddle-like structure which is probably caused by the bulky mesityl groups. Introduction of two BN units notably narrowed the HOMO–LUMO band gap with a higher HOMO level and a lower LUMO level compared to those of coronene. Compared to its carbonaceous analogue, **28** had significantly red-shifted absorption bands and blue-shifted emission bands. The intensities of both absorption and emission as well as the fluorescence quantum yield of **28** were remarkably enhanced.

The Zhang group and the Pei group independently discovered the synthesis of (BN)<sub>3</sub>-doped coronene **29** (Fig. 9b).<sup>89,90</sup> The backbone of **29** demonstrated a fully planar geometry. The longer B=N double bond and shorter C–N single bonds were ascribed to the significant  $\pi$ -electron delocalization in the crystal structure of **29**. The HOMO–LUMO band gap was further enlarged with an increased LUMO level and a decreased HOMO level.

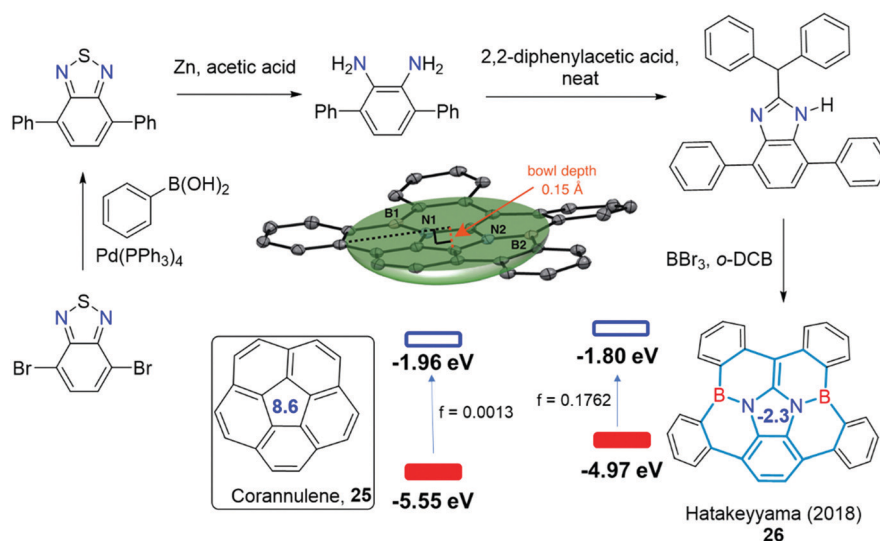


Fig. 8 Synthesis of (BN)<sub>2</sub>-embedded corannulene. The inset shows the bowl depth of the crystal structure of **26**. The crystal structure of **26** reprinted with permission from ref. 86. Copyright 2018 American Chemical Society.

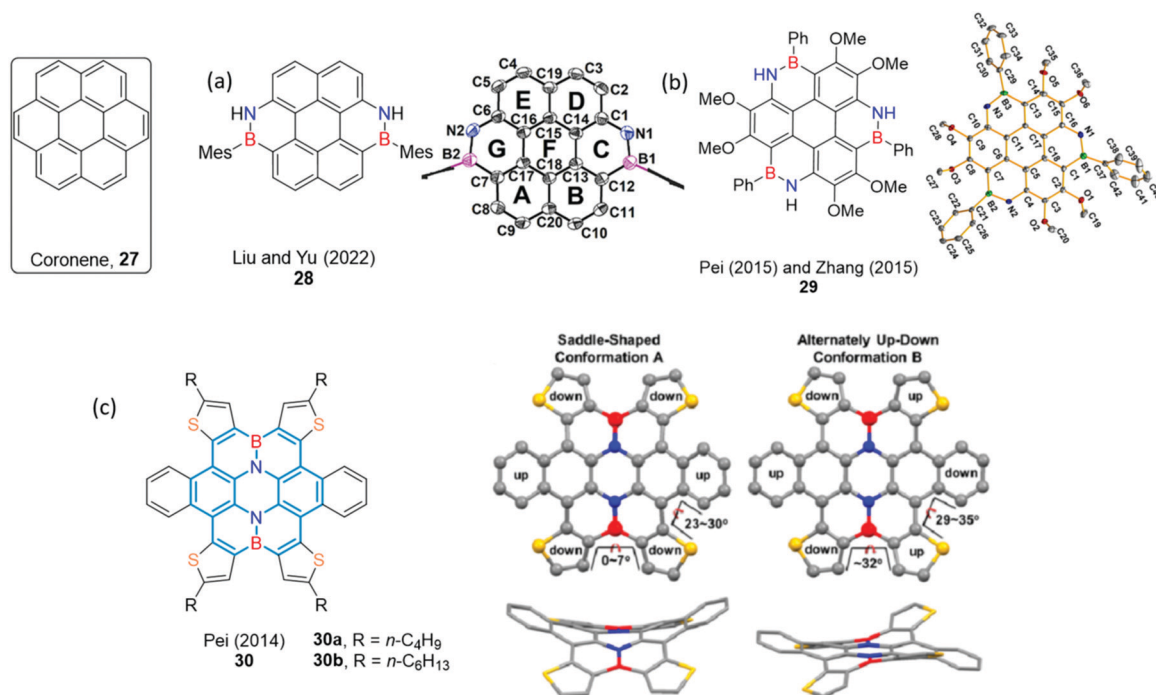


Fig. 9 Multi-BN-doped coronene and its derivatives. Crystal structures of **28** reprinted with permission from ref. 88. Copyright 2022 American Chemical Society. Crystal structures of **29** reprinted with permission from ref. 89. Copyright 2015 American Chemical Society. Crystal structures of **30b** reprinted with permission from ref. 21. Copyright 2014 American Chemical Society.

The absorption and emission spectra were notably blue-shifted, while the quantum yield of **29** was considerably higher than that of **27**. The stability of **29** toward moisture was studied by Zhang *et al.*; **29** underwent the deprotection of boron atoms with the formation of borinic acids. On comparing the bis-BN-doped coronene **28** to tri-BN-doped coronene **29**, compound **28** had a smaller HOMO–LUMO energy level and smaller Stokes shift than its all-carbon analogue, while compound **29** had a wider HOMO–LUMO band gap and larger Stokes shift than its carbonaceous coronene.

As continued interest in BN-PAHs with thiophene moieties, Pei *et al.* disclosed the synthesis of bis-BN-doped  $\pi$ -conjugated systems with four thiophenes (**30** in Fig. 9c).<sup>21</sup> A rare phenomenon for PAHs which contained two different conformers (saddle-shaped conformation and alternately up–down conformation)

in the single crystal was observed (Fig. 9c). The two conformers were self-assembled into a sandwich structure and further formed a  $\pi$ -stacking column. Doping BN units did not change the HOMO–LUMO band gap too much with a 0.1 eV lower HOMO level and an unchanged LUMO level. The packed microribbons were investigated to be a good charge transport material with superior photoconductivity.

Coronene diimides (CDIs, **31** in Fig. 10) have blue-shifted absorption maxima and lower quantum yields compared to PDIs.<sup>91,92</sup> Hissler, Staubitz *et al.* discovered a synthetic route for using 1,7-dibromo-PDIs as starting materials to achieve bis-BN-doped CDIs **32**.<sup>93</sup> Doping two BN units at the edge of the CDIs resulted in large bathochromically shifted absorption with higher molar extinction coefficients, narrow Stokes shifts and significantly higher quantum yields compared to its carbonaceous CDIs.

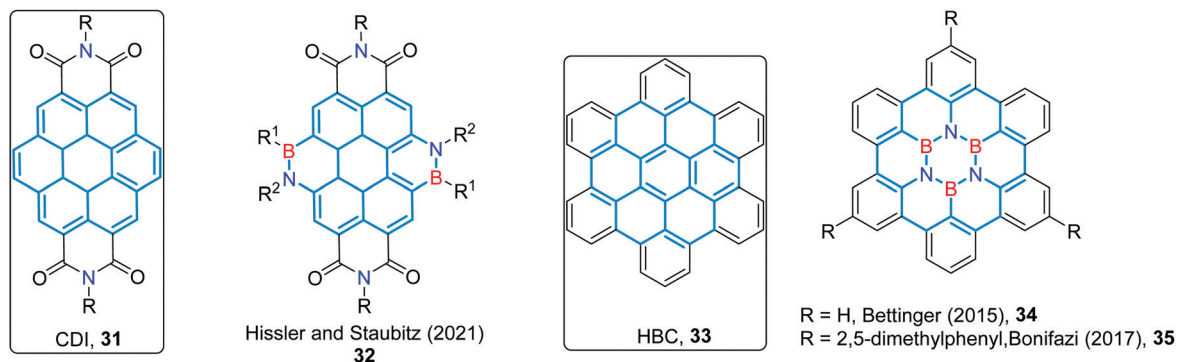


Fig. 10 Multi-BN-doped CDI, HBC and their derivatives.



The different substituents on nitrogen atoms did not impact the optical properties at the single molecule level, but substantially influence optical properties and performance in OLEDs and OFETs in the solid state.

As the further conjugation extension of coronene, hexa-*peri*-hexabenzocoronene (HBC, **33** in Fig. 10) has been mainly studied in supramolecular electronics.<sup>94–103</sup> The isolation of the first BN center-doped HBC **34** was achieved as a minor product by Bettinger and coworkers *via* pyrolysis of the borazino precursor at 550 °C, accompanying the major product tetraaza-tetraborocine derivative **37** (Fig. 11a).<sup>104</sup> Scanning tunneling microscopy (STM) was exploited to confirm that (BN)<sub>3</sub>-HBC **34** lay on a Au(111) surface in a 2D pattern. The thermolytic process highly depended on the temperature. If the temperature of thermolysis was decreased to 400–410 °C, only borylated product **36** as well as a small amount of **37** was obtained. The poor solubility of BN-HBC **34** limited further structural and optoelectronic studies in solutions. Bonifazi *et al.* documented the first rational synthesis of (BN)<sub>3</sub>-HBC **35**, which started from the formation of a (BN)<sub>3</sub>-core and fused six C–C bonds through intramolecular Friedel–Crafts-type reactions (Fig. 11b).<sup>105</sup> 2,5-Dimethylphenyl groups were used to improve the solubility. In this example, almost all the photophysical properties dramatically changed after BN units were introduced. The maxima of absorption, fluorescence and phosphorescence in solutions were ~80 nm blue-shifted compared to those of its all-carbon analogue. The optical gap of BN-HBC **35** was *ca.* 0.53 eV larger than that of its carbonaceous structure. The fluorescence decays of **35** were slightly shorter than those of its all-carbon analogue both in solution and in the solid state, while the lifetime (4.0 s) of phosphorescence of **35** at 77 K in solution was 5-fold longer compared to the 2,5-dimethylphenyl group substituted HBC.

While more and more attention has been paid to construction of BN-PAHs, researchers are also focusing on these PAHs which themselves have not been synthesized. Recently, the tetrabenzofused pyrene, which is also named ixene **38**, and its BN partially edge-doped derivative **39** were synthesized by Lee, Shin, Park and

coworkers (Fig. 12).<sup>106</sup> For the synthesis of **38** and **39**, a double annulation reaction was exploited, and then an intramolecular C–H bond arylation with aryl chloride was used to achieve the fusion of the two final phenyl rings. The crystal structure of **39** revealed a planar pyrene core, while the four peripheral phenyl rings were distorted, which was consistent with STM studies. The lengths of the BN bonds in **39** were shorter than those previously reported BN edge-doped-PAHs, which emphasizes the importance of BN units' locations. With respect to the optoelectronic properties, due to the smaller HOMO–LUMO gap, both the absorption and emission spectra of BN-ixene **39** displayed *ca.* 20 nm red-shift with a doubled quantum yield compared to those of ixene **38**, while cyclic voltammetry indicated that the smaller HOMO–LUMO band gap resulted from the lower LUMO of **39**.

Doping two BN units into the helical dibenzo[*a,m*]rubicene (DBR) was achieved by Shang and Nakamura *et al.* *via* the construction of diphenylindolocarbazole **41a** followed by double electrophilic borylation (Fig. 13).<sup>107</sup> The six-membered rings with the BN units in **41** changed from aromatic to non-aromatic, while the aromaticity of the five-membered rings with the BN units in **41** trended in the opposite direction. Compared to DBR **40**, BN-doped DBR **41** exhibited a larger optical gap with blue-shifted absorption and emission bands and a much smaller Stokes shift. The photoluminescence quantum yield of **41** was substantially increased up to 88%. In addition, BN-DBR **41** showed rich color tunability induced by coordination with the fluoride anion.

## 2.2 BN-doped ladder-type acenes

Ladder-type acenes usually refer to PAHs made up of linearly fused aromatic rings.<sup>97,108,109</sup> This class of molecules usually features rigid planar backbones, unique photophysical properties and self-assembly behaviors, as well as attractive charge transport properties.<sup>5,33,110–114</sup>

Dibenzo[*a,e*]pentalene (DBP, **42**) is a ladder-type molecule consisting of two antiaromatic five-membered rings and two phenyl rings (Fig. 14).<sup>115,116</sup> The investigation of the effect of BN

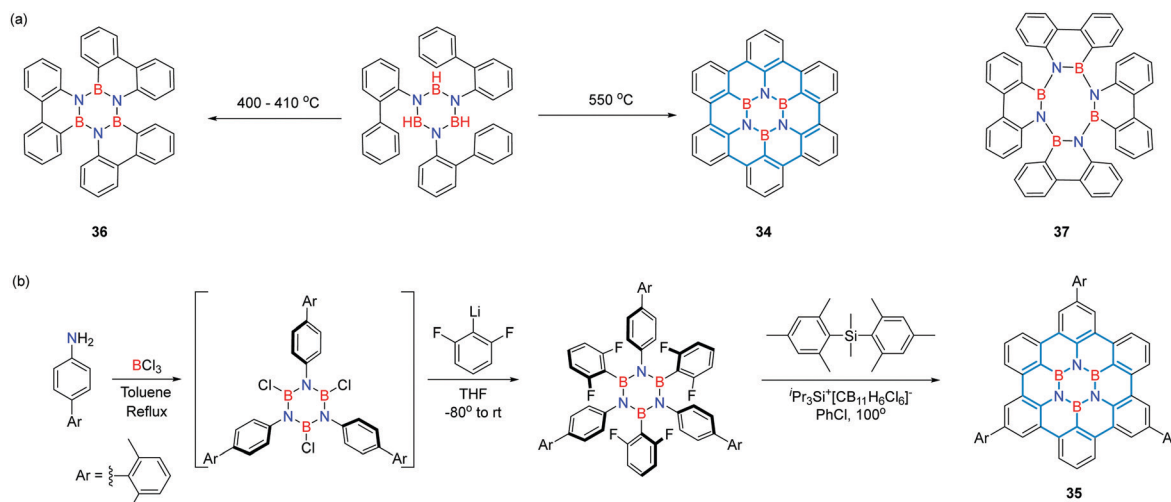


Fig. 11 Synthesis of (BN)<sub>3</sub>-HBCs.

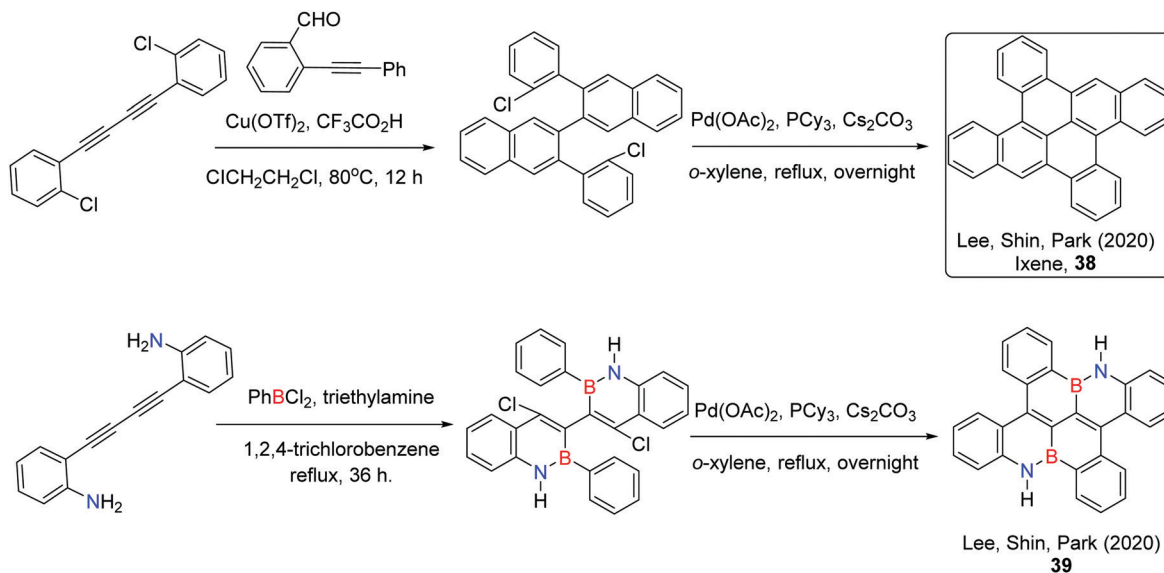


Fig. 12 Synthesis of ixene and its bis-BN-doped derivative.

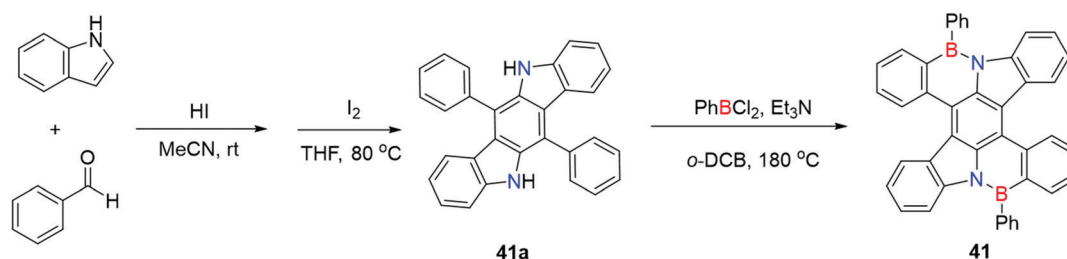
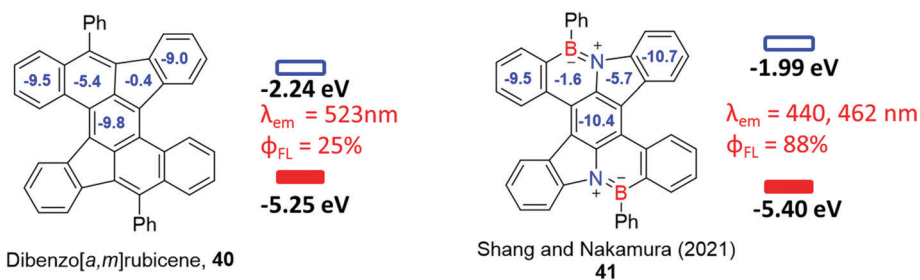


Fig. 13 (BN)<sub>2</sub>-doped dibenzo[*a,m*]rubicene.

units' substitution on the aromaticity and photophysical properties of BN-DBPs **43** and **44** was reported by Feng, Müllen and coworkers.<sup>29</sup> The synthesis of BN-DBP **43** started with the formation of 2,2'-dibromohydrazobenzene from reduction of 1-bromo-2-nitrobenzene, following a <sup>t</sup>BuLi-assisted double borylation reaction (Fig. 14b). 2-Bromophenylboronic acid was exploited to construct the first BN five-membered ring, then the <sup>t</sup>BuLi-assisted double borylation reaction was once again utilized to achieve BN-DBP **44**. As expected, the skeletons of **43** and **44** were planar in the crystal structures. With respect to aromaticity, NICS(1) study indicated that doping BN units could make the two phenyl rings of both **43** and **44** have higher

aromaticity, while the pentalene core of BN-DBP **43** changed from antiaromatic to almost nonaromatic and the BNB 5-membered ring in **44** was still antiaromatic. Different doping patterns also affected the frontier molecular orbitals with higher LUMOs and lower HOMOs. The nonnegligible role of the orientation of multiple BN units in  $\pi$ -conjugated molecules was stood out by the totally different emission properties, in which the center-symmetric BN-DBP **43** exhibited fluorescence at  $\lambda_{em} = 403$  with a quantum yield of 18%, while the unsymmetric **44** was non-emissive. Meanwhile, Cui and coworkers independently reported the BN-benzopentalene **46**, which showed a larger HOMO–LUMO band gap than that of its carbonaceous

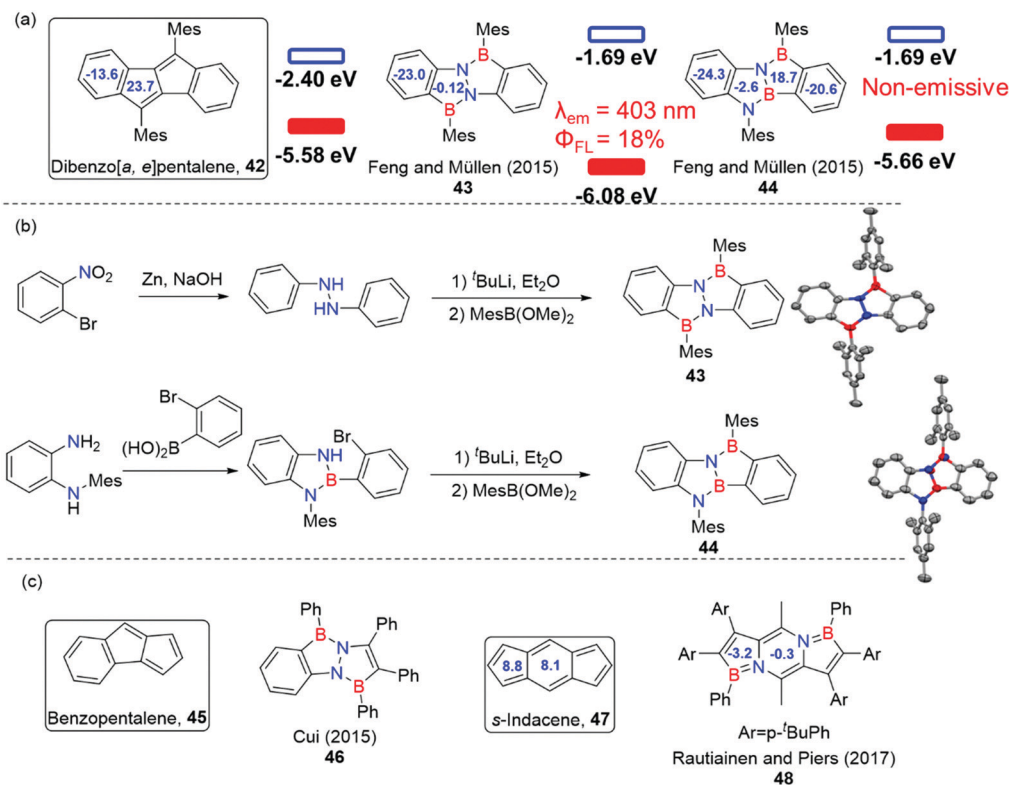


Fig. 14 (BN)<sub>2</sub>-Dibenzo[*a, e*]pentalenes. Crystal structures of **43** and **44** reprinted with permission from ref. 29. Copyright 2015 American Chemical Society.

benzopentalene **45** (Fig. 14c).<sup>117</sup> In 2017, Rautiainen and Piers *et al.* developed zirconocene-based methods for the preparation of BN-indenes **48**, in which the aromaticity of the five- and six-membered rings shifted to nonaromatic compared with that of **47**.<sup>118</sup>

Peripheral benzenoid rings of tetrabenzopentacene (TBP) have been introduced to increase the stability. Although the stability of TBP indeed showed improved stability compared to pentacene, it is still prone to decompose. Wang, Pei and coworkers reported BN-doped TBP **50** with improved stability compared to the carbonaceous analogue **49** (Fig. 15a).<sup>119</sup> Bis-BN-doped **50** exhibited exceptional stability toward air, moisture, light and heat, which could easily cause the decomposition of large acenes. The high stability was ascribed to the decreased HOMO energy level after two BN units were introduced into TBP. With respect to the synthesis of **50**, the precursor compound **50b** was synthesized from several steps of C–C bond cross coupling reactions and deprotection reactions, borylative cyclization was utilized to access the precursor **50a**, and the two end rings of product **50** were finally sealed by a UV-light-mediated radical cyclization reaction. The high stability of the bis-BN-doped TBP **50** enabled achieving p-type OFETs with mobilities of up to 0.33 cm<sup>2</sup> V<sup>-1</sup> s<sup>-1</sup>.

As a U-shape ladder-type acene, dibenzo[*a, o*]picene (DBP, **51**) has intriguingly predicted structural and electronic properties (Fig. 15b).<sup>120,121</sup> Although the synthesis of DBP has not been achieved, Piers *et al.* reported the synthesis of bis-BN-doped DBP *via* the methodology developed before,<sup>48,57,122–126</sup> where the diethynylbenzene **52a** reacted with a slightly excess of the boracycle **52b**, followed by the elimination of TMSCl and

cycloisomerization of the pendant alkynes.<sup>125</sup> The boracycle **52b** could be used in other types of BN partially edge-doped PAHs and BN center-doped PAHs. NICS(1) calculations indicated that all the rings in BN-DBP **52** were aromatic.

The BN-doped ladder-type molecules linked through a central benzene ring with different BN orientations have been extensively studied (Fig. 16). Zhang, Feng and coworkers successively studied the synthesis and optoelectronic applications of ladder molecules **53** and **54** that have different terminal aromatic rings and BN orientations.<sup>127,128</sup> Compared to **53**, both the absorption and emission bands of **54** showed about 30 nm blue-shift with improved quantum yields. Compound **53** had been demonstrated as host materials in blue OLEDs. As the isomers of **53** and **54**, compound **55** and **56** were angular with syn-located BN units.<sup>129</sup> The different orientations of ladder molecules **53** and **55** as well as **54** and **56** had a negligible impact on the maximum wavelengths of absorption and emission, but on switching the bilateral aromatic rings from thiophene to benzene in **55** and **56**, the absorption and emission were blue shifted *ca.* 30 nm. Due to their rigid structures, **53–56** showed very small Stokes shifts. Compared to **53** and **55**, compound **57** displayed blue-shifted absorption and emission.<sup>130</sup> The benzothiadiazole segment in **58** significantly moved the absorption and emission toward longer wavelengths with a very large Stokes shift (95 nm).<sup>130</sup> Although compounds **59** and **60** had different orientations from **55** and **56**, the photo-physical properties did not show noteworthy changes.<sup>131</sup>

Gryko *et al.* reported a simple synthetic approach to ladder-type diazabenzoindoles **61** and bis-BN-benzoindoles **62** (Fig. 17).<sup>132</sup> Different from the NN unit doped **61**, BN-heteroacene **62** exhibited

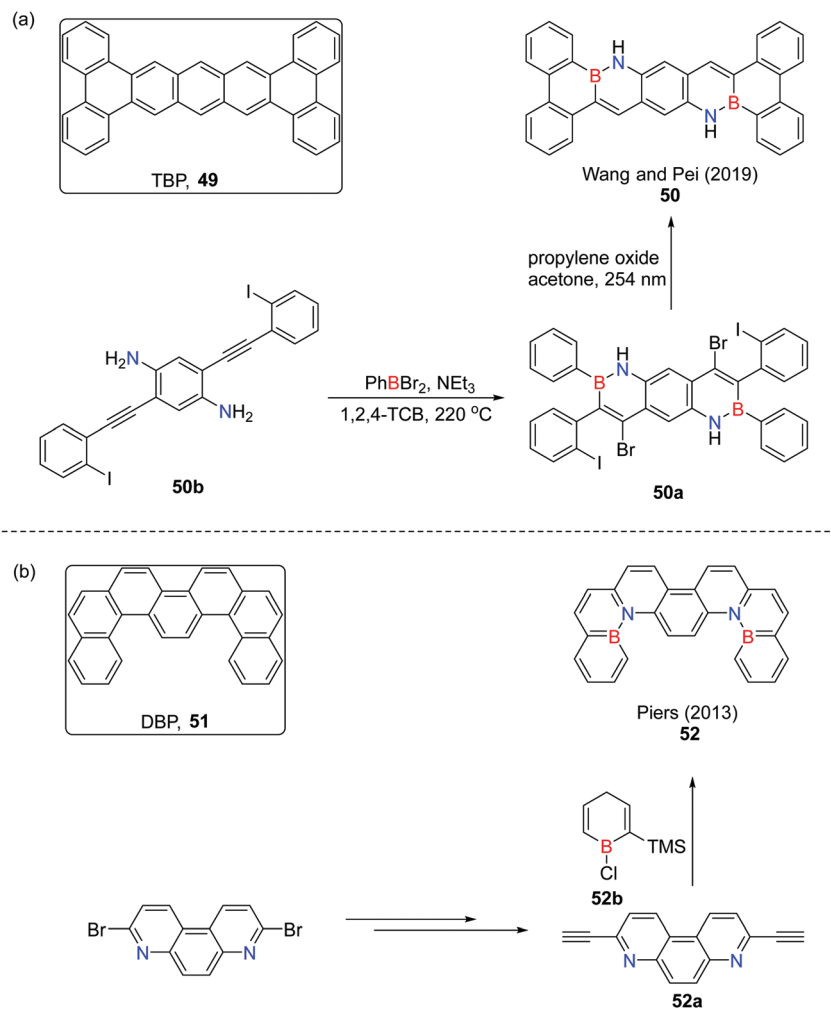


Fig. 15 (a) Tetrabenzopentacene (TBP) and bis-BN-doped TBP, and (b) dibenzo[*a,o*]picene (DBP) and bis-BN-doped DBP.

a large blue-shift of absorption with a high molar absorption coefficient. In addition, **62** was highly fluorescent with a quantum yield of 70%. The non-emissive properties of **61** were likely caused by the nonradiative decay because of the diazine scaffold. Changing the central aromatic core from pyrolopyrrole in **62** to thienothiophene in **63** did not substantially change the photophysical properties; however, tailoring the orientation of the central thienothiophene made the absorption and emission bands of **64** *ca.* 20 nm blue-shifted compared to **63**.<sup>128</sup> Two azaborine-thiophene ladder-type heteroacenes **65** and **66** with a central thieno core were reported by the Per-pichka group (Fig. 18).<sup>133</sup> Both **65** and **66** showed highly rigid structures and deep-blue fluorescence. The existence of the linker between two nitrogen atoms did not notably shift the photophysical properties. Changing the bilateral aromatic rings from thiophene to benzene substantially moved the absorption and emission bands of **67** toward shorter wavelengths. Manipulating the BN units' arrangement from tail-to-tail to head-to-head did not have a noteworthy effect on the photophysical properties of **67** and **68**.<sup>31</sup> Thiophene has been widely used as segments of BN-doped PAHs. This is mainly due to the

high reactivity of C–H bonds in thiophene, which makes electrophilic borylation easier.

Chen and coworkers reported a series of BN-functionalized benzotrithiophene-based azaborines with different numbers of BN units prepared *via* electrophilic borylation (Fig. 19).<sup>134</sup> Surprisingly, the patterns of the absorption spectra of these three compounds were nearly identical with different molar absorption coefficients. The maximum wavelength of fluorescence was only 5 nm red-shifted with the increase of BN units. Compounds **69–71** showed red-shifted absorption and emission upon fluoride titration.

PAHs bridged with the BN unit were investigated as charge transport materials by Hatakeyama, Seki and Nakamura in 2011 (Fig. 20).<sup>135</sup> Compared to the superior hole mobility of **72a**, they only reported the synthesis of bis-BN-doped PAHs **72** without investigation of charge transport properties, which was believed to be also suitable for organic electronics. Xing, Zhu and Cui reported a transition-metal catalyzed synthesis of the ladder-type acene **73** with central oxepin cores (Fig. 20).<sup>136</sup> This type of ladder molecule exhibited dually-fluorescent emissions. The tunable emission colors of **73** could be achieved by

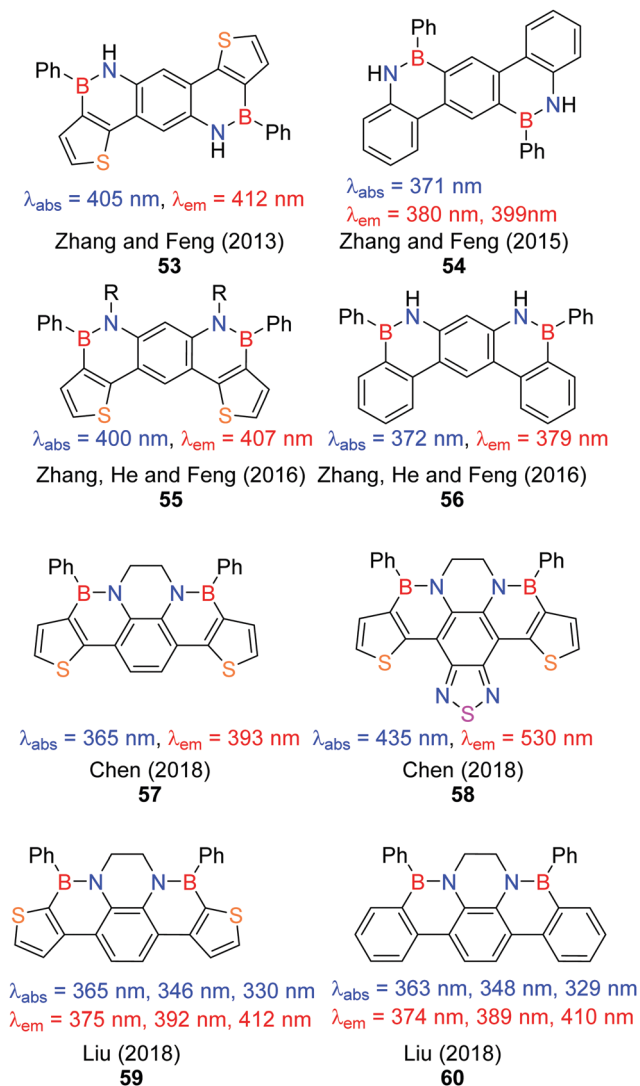


Fig. 16 Representative examples of bis-BN-doped ladder-type molecules linked with a benzene.

manipulating the ratio of solvents, the concentration of solution, or temperature. Integrating highly dipolar azulene into BN-PAHs was also studied (Fig. 20).<sup>137</sup> Compared to mono-BN-doped molecule **74a**, the bis-BN-doped ladder molecule **74** showed red-shifted absorption with a higher molar absorption coefficient. Both compounds **74a** and **74** had very low quantum yields of fluorescence, while the fluorescence of **74a** and **74** originated from the non-lowest excited states. Compared to their carbonaceous analogues, introducing BN units could lower the HOMO level and keep the LUMO unchanged.

### 2.3 NBN-doped PAHs

Introduction of NBN units into PAHs was initially exploited to increase the stability of PAHs and nanographenes through BN edge doping.<sup>138–140</sup> Now the NBN unit is not only doped at the edge of PAHs, but also embedded into the center of PAHs. There are several examples of mono-NBN-doped PAHs, which will not be discussed if they do not have multi-BN-doped analogues.<sup>138–145</sup>

Feng *et al.* discovered the synthesis of a series of mono-NBN and bis-NBN edge-doped PAHs with a central phenalene (Fig. 21).<sup>146</sup> The NBN unit significantly enhanced the stability of NBN-PAHs compared to their all-carbon analogues. The chemical oxidation of **76** resulted in a dimer of **76** by  $\text{Cu}(\text{OTf})_2$ . The bis-NBN-doped PAH **77** showed largely red-shifted absorption and emission due to the larger conjugation with a significantly enhanced quantum yield compared to mono-NBN-doped PAH **76**. As continued interest in NBN-PAHs, the same group recently demonstrated the introduction of two NBN units into bis-tetracene **78** and *peri*-tetracene **80** (Fig. 22).<sup>147–149</sup> The bis-NBN-doped bis-tetracene **79** was obtained by electrophilic borylation of the tetraamine substrate using highly Lewis acidic  $\text{BI}_3$ . The further fusion of **79** using traditional in-solution cyclization did not succeed in accessing BN-*peri*-tetracene **81**, which was achieved by surface-assisted intramolecular cyclodehydrogenation. The structure of **81** was further characterized by high resolution mass spectrometry (HRMS) and noncontact atomic force microscopy (nc-AFM). The excellent stability of BN-bis-tetracene **79** and BN-*peri*-tetracene **81** was ascribed to the doubled energy gap compared with their carbonaceous bis-tetracene **78** and *peri*-tetracene **80**. For the NBN-PAHs with two NBN units, the differences between bis-NBN-doped PAH **77** and bis-BN-doped-*peri*-tetracene **81** were mainly attributed to the fact that **81** had a smaller optical gap. In addition, helical **79** underwent stepwise chemical oxidation to generate the corresponding radical cation and dication.

The first  $(\text{NBN})_3$ -[4]triangulene **82** was reported by the Miao group through a threefold electrophilic borylation reaction (Fig. 23).<sup>150</sup> The crystal structure of **82** showed that it was slightly bent with dihedral angles of about  $5.7^\circ$  between peripheral benzenoid rings. NICS(1) studies showed that the benzenoid rings at the periphery and centers of **82** exhibited aromaticity, while BN-benzenoid rings showed non-aromaticity. The unprotected NBN units provided a dual hydrogen-bond donor, which could form a 2D network with a twofold dual-hydrogen bond acceptor (TDHBA) like 2,7-di(*tert*-butyl)-pyrene-4,5,9,10-tetraone (Fig. 23). In addition, the hydrogen-bonding between **82** and some hydrogen acceptors could result in a change in fluorescence. Recently, multiple NBN center-doped triangulene was theoretically investigated.<sup>151</sup>

New methodologies to construct BN-PAHs are always highly desired. Electrophilic borylation cyclization is one of the most used methods to build BN-rings. The methodologies for forming BN-rings after introducing BN units are quite limited. Recently, Ma and Zhao *et al.* developed a palladium-catalyzed Larock-type cyclization of NBN-pentagons and hexagons with acetylenes (Fig. 24);<sup>152</sup> this methodology was also successfully exploited to construct large ladder-type acene **83** with two NBN units. The twisted geometry of **83** could undergo photoinduced structural planarization (PISP) with changes in color and quantum yield in solutions once the concentrations were changed.

### 2.4 BN-doped oligomers

Oligomers, molecules consisting of a few similar or identical repeating units, have been extensively studied. Due to the

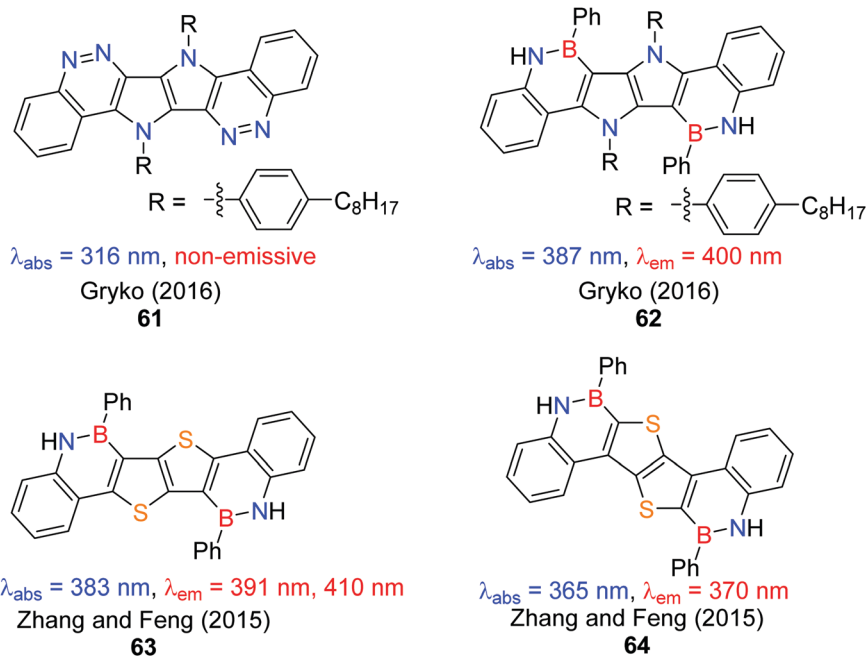


Fig. 17 Representative examples of bis-BN-doped ladder-type molecules linked with heteroaromatic rings.

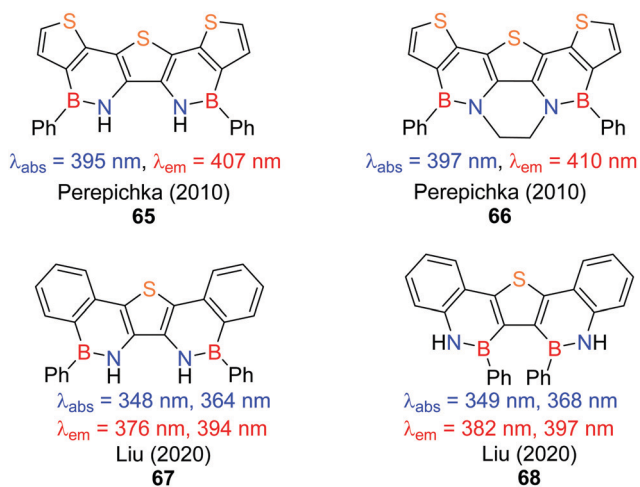


Fig. 18 Representative examples of bis-BN-doped ladder-type molecules linked with a thiophene.

difficulty of introducing multiple boron atoms at once, the research of oligomers with multiple BN units is relatively scarce.<sup>153</sup>

Based on an extensive study on the selective functionalization of 1,2-azaborines, Liu and Jäkle collaborated the first regioregular synthesis of azaborine oligomers **85** and **86** as well as the corresponding azaborine polymer **87** (Fig. 25).<sup>154</sup> The crystal structure of dimer **85** exhibited a nearly coplanar *syn* arrangement of the heterocycles, which was partially contributed by N-H... $\pi$  interactions. The lowest-energy absorption peaks of **84** ( $\lambda_{\text{abs}} = 277 \text{ nm}$ ), **85** ( $\lambda_{\text{abs}} = 334 \text{ nm}$ ), **86** ( $\lambda_{\text{abs}} = 383 \text{ nm}$ ) and **87** ( $\lambda_{\text{abs}} = 457 \text{ nm}$ ) exhibited a substantial bathochromic shift as the

conjugation of the backbone was extended. The molar absorption coefficients of dimer **85** and trimer **86** were two-fold and three-fold that of monomer **84**, respectively. However, the polymer **87** had a lower molar absorption coefficient than the monomer **84**. The maximum of emission moved toward the long wavelength region from the oligomer **85** ( $\lambda_{\text{em}} = 411 \text{ nm}$ ) and **86** ( $\lambda_{\text{em}} = 491 \text{ nm}$ ), to polymer **87** ( $\lambda_{\text{em}} = 600 \text{ nm}$ ), though the monomer **84** was not fluorescent.

Recently, Zhou and coworkers reported a series of BN-doped PAHs with peripheral thiophenes **88–91** (Fig. 26).<sup>155</sup> The electron-rich properties of the thiophene moiety are ascribed to the successful embedding of multiple BN units *via* electrophilic borylation. The B–N bond length (1.4555 Å) in the crystal structure of monomer **88** was between the B–N single bond (1.58 Å) and the localized B=N double bond (1.40 Å), which indicates that the BN bond was delocalized due the effective conjugation extension through the BN bond. Although both the absorption and emission bands of these compounds **88–91** displayed red-shift as the conjugation was extended, the red-shifts among **89–91** were negligible. The optical band gaps of these molecules also decreased following the order of **88** to **91**. The aromaticity and intramolecular charge transfer of these four BN-PAHs were significantly impacted by chemical oxidation.

In order to investigate the influence of the BN/CC isosterism on the cation- $\pi$  binding ability, Liu *et al.* exploited the BN-doped indole as the building block to synthesize the oligomer **93** (Fig. 27).<sup>156</sup> Nuclear magnetic resonance (NMR) monitored titrations with cations  $\text{Li}^+$  and  $\text{K}^+$  showed that embedding BN units into the indole only marginally decreased the cation- $\pi$  binding ability compared to its carbonaceous triindole **92**.

BN-aromatic rings are often achieved by either electrophilic borylation or transition-metal catalyzed cyclization. Breaking

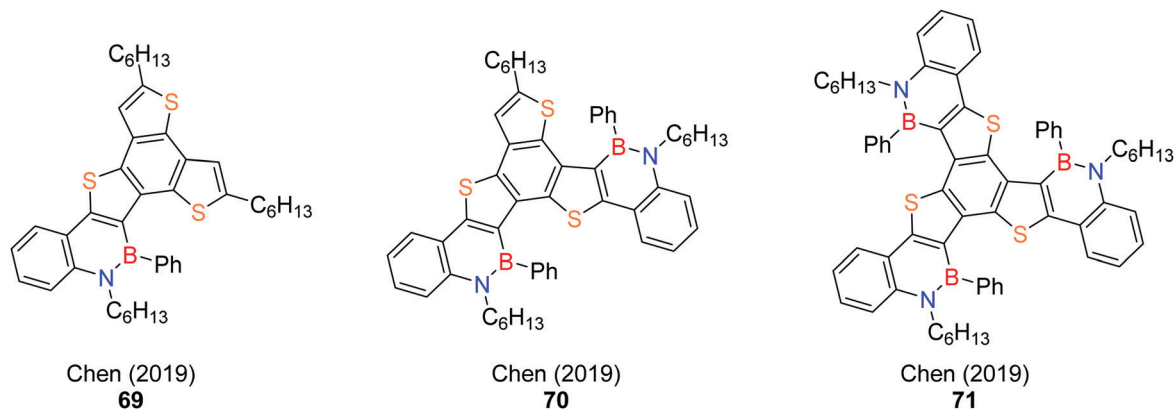


Fig. 19 BN-functionalized benzotrithiophene-based azaborines.

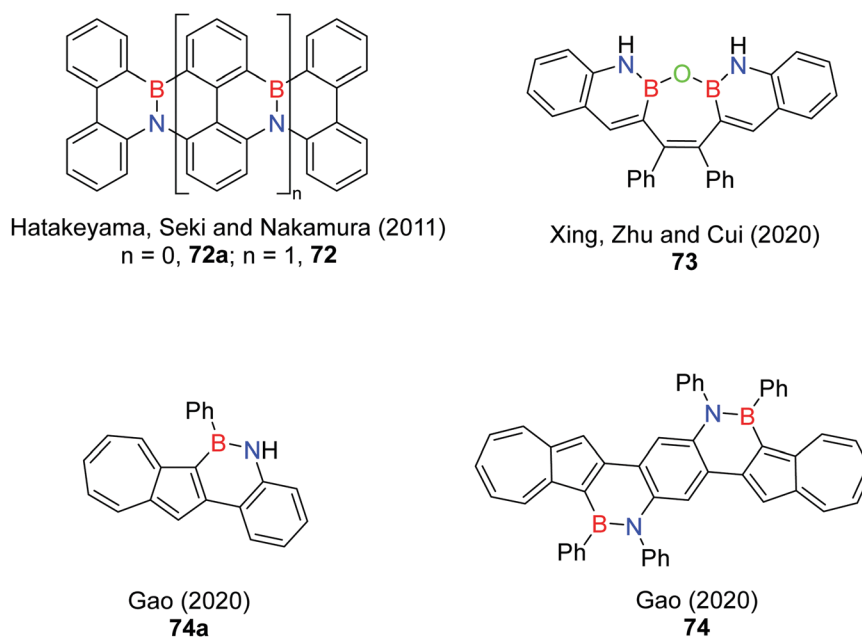


Fig. 20 Selective examples of other types of BN-doped ladder-type acenes.

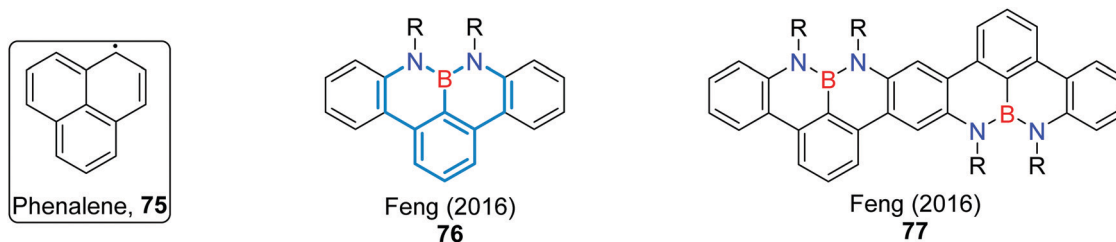


Fig. 21 NBN edge-doped PAHs with a phenalene core.

aromatic rings is regarded as a hardly accessible approach. Recently, Yorimitsu and coworkers developed a brand-new strategy for constructing BN-naphthalene derivatives *via* a lithium-mediated reductive ring-opening reaction of indole derivatives followed by a boron insertion reaction (Fig. 28).<sup>157</sup>

A variety of BN-naphthalene derivatives were obtained under the developed conditions. Even oligomers **94**, **95** and **97** could be accessed using the same conditions. The dimer **95** further underwent transition-metal catalyzed cyclization, forming the bis-BN-doped ladder-type acene **96**. Compound **96** had the absorption

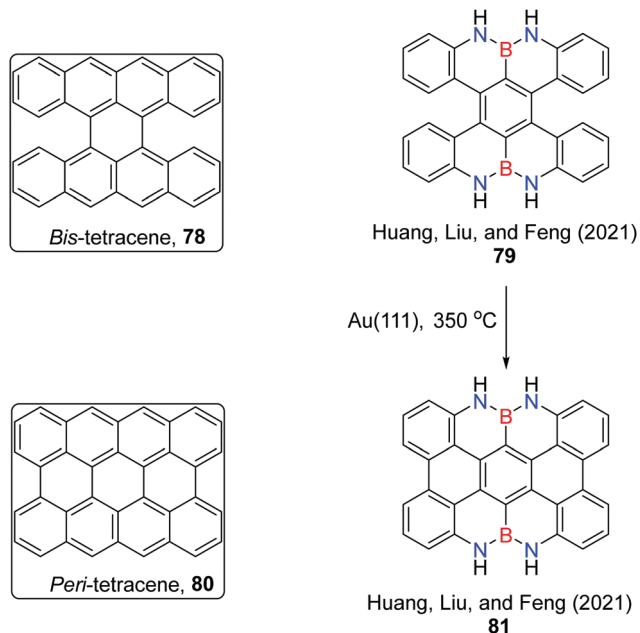


Fig. 22 NBN-doped *bis*-tetracene and *peri*-tetracene.

maximum at  $\lambda_{\text{abs}} = 387$  nm and emission maxima at  $\lambda_{\text{em}} = 400$  and 419 nm with a quantum yield of 19%. The photophysical properties of the remaining BN-PAHs obtained through this approach were not reported, but this new synthetic strategy provides an alternative scenario for construction of BN-PAHs.

### 3. Multi-BN-doped $\pi$ -conjugated systems with discrete boron and nitrogen atoms

BN-doped benzenes with discrete boron and nitrogen atoms are also named 1,3-azaborines and 1,4-azaborines. Due to the

scarcity of 1,3-azaborine derivatives, this section will focus on 1,4-azaborines. Studying 1,4-azaborines has a long history;<sup>158–160</sup> however, the renaissance in the study of 1,4-BN-PAHs was ignited until Hatakeyama and coworkers introduced multi-resonant thermally activated delayed fluorescence (MR-TADF) molecules in 2016.<sup>23</sup>

#### 3.1 1,4-BN-PAHs without MR-TADF

In 2006, Kawashima and coworkers explored the incorporation of anthracene, pentacene and heptacene with the aim of providing emitting materials for OLEDs (Fig. 29).<sup>27</sup> The 1,4-BN-anthracene **98** and the ladder-type molecules **99–101** were synthesized in high yields through lithium–bromide exchange of the corresponding precursors followed by addition of MesB(OMe)<sub>2</sub>. The crystal structure of para-type compound **99** exhibited a nearly planar bis-BN-doped pentacene core. No obvious intermolecular interactions in the crystalline state of **99** were observed likely due to the bulky mesityl groups on the boron atoms. Compared to the 1,4-BN-anthracene **98**, bathochromically-shifted absorption and fluorescence maxima were observed for para-type BN-pentacene **99** and tri-BN-heptacene **101** by extending the  $\pi$ -conjugation using ladder-type frameworks. However, the absorption and emission bands of meta-type BN-pentacene **100** were only slightly red-shifted compared with those of **98**, probably due to the weak  $\pi$ -conjugation between the two fused azaborine units in the syn-parallel orientation mode. The distinct absorption and emission spectra of para-type BN-pentacene **99** and meta-type BN-pentacene **100** indicate that even incorporating BN units with different orientations in the same carbonaceous PAHs could result in dissimilar photophysical properties.

A variety of thieno-fused ladder-type 1,4-BN-acenes have been reported by Mitsudo and Suga *et al.* using a Friedel–Crafts-type C–H borylation to introduce boron atoms (Fig. 30).<sup>161</sup> Compared to the 1,4-BN-acenes in Fig. 28, the thieno-fused molecules **102** and **103** only exhibited weak fluorescence ( $\Phi < 0.1$ ), indicating

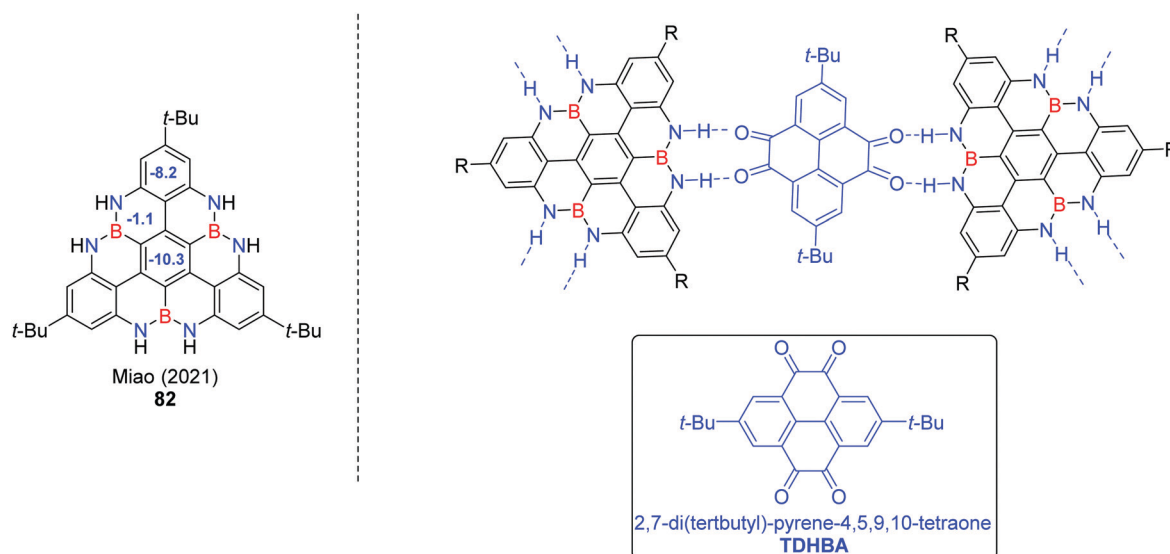


Fig. 23 (NBN)<sub>3</sub>-[4]triangulene **82** and the proposed hydrogen-bonded 2D network of **82** and TDHBA.



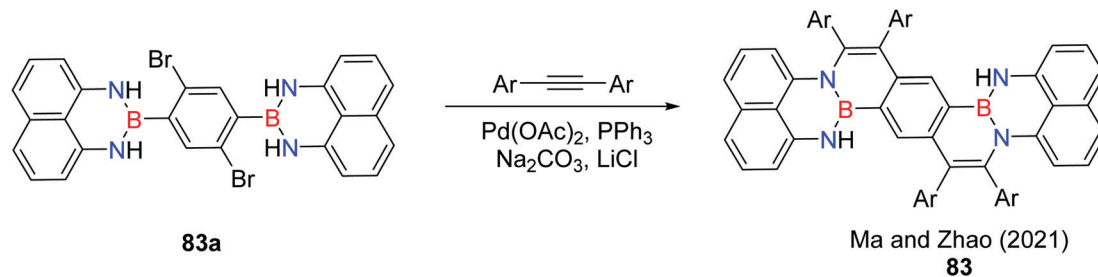


Fig. 24 Construction of the bis-NBN-ladder-type acene.

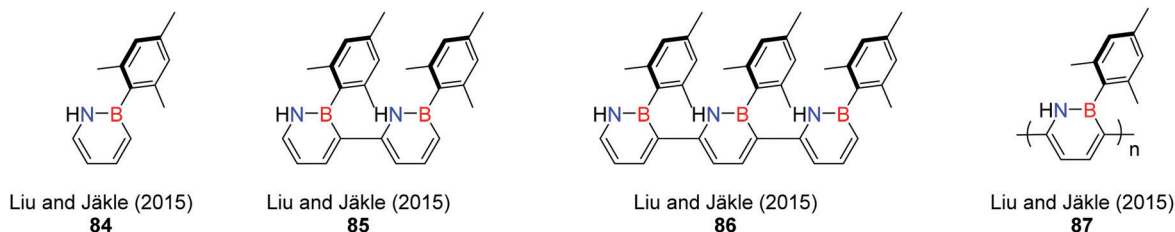


Fig. 25 1,2-Azaborine oligomers.

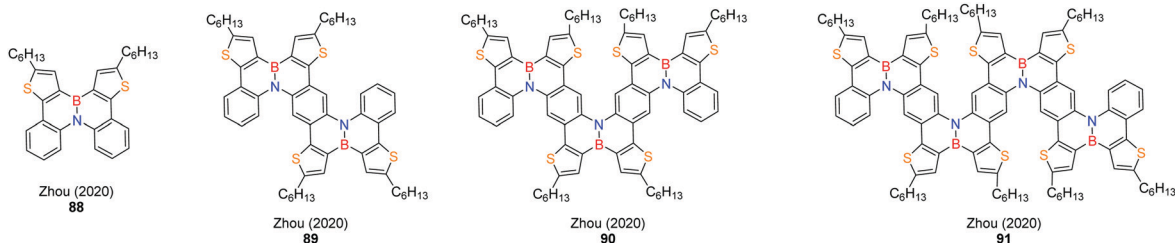
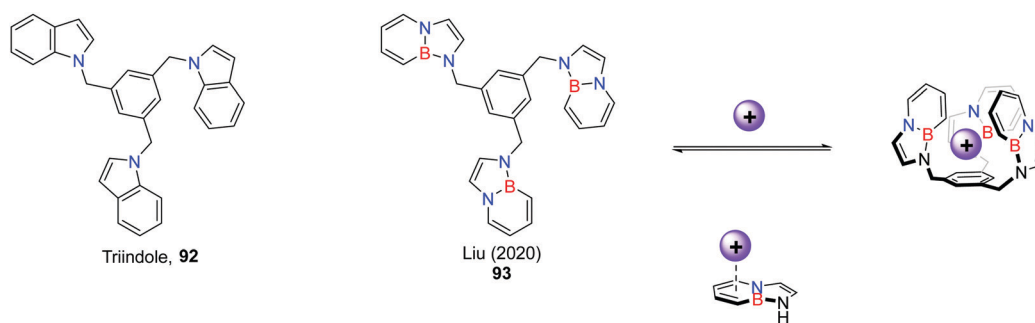


Fig. 26 BN-PAH oligomers with peripheral thiophenes.

Fig. 27 Oligomer of BN-indole and its cation- $\pi$  binding ability. Reproduced from ref. 156 with permission from The Royal Society of Chemistry.

that fusing benzo and thieno rings with 1,4-azaborines could cause substantial changes in photophysical properties. Not surprisingly, the ladder-type thieno-acene **103** showed a red-shifted absorption onset compared to the dithieno-1,4-azaborine **102**.

Atom-specifically substituting graphene nanoribbons (GNRs) could be achieved by so-called “bottom-up” synthesis.<sup>162–165</sup> Starting from BN-doped anthracene derivative **104b**, Kawai,

Hatakeyama and Foster *et al.* developed an on-surface chemical synthesis strategy involving halide-halide coupling cyclodehydrogenation reactions (Fig. 31), which was used to access the series BN-GNR **104** bearing one BN unit in its repeating unit, and the alternative BN-GNR **105** that had two BN units in its repeating unit.<sup>166</sup> The elemental differences in the GNRs were resolved by AFM with a CO-functionalized tip.

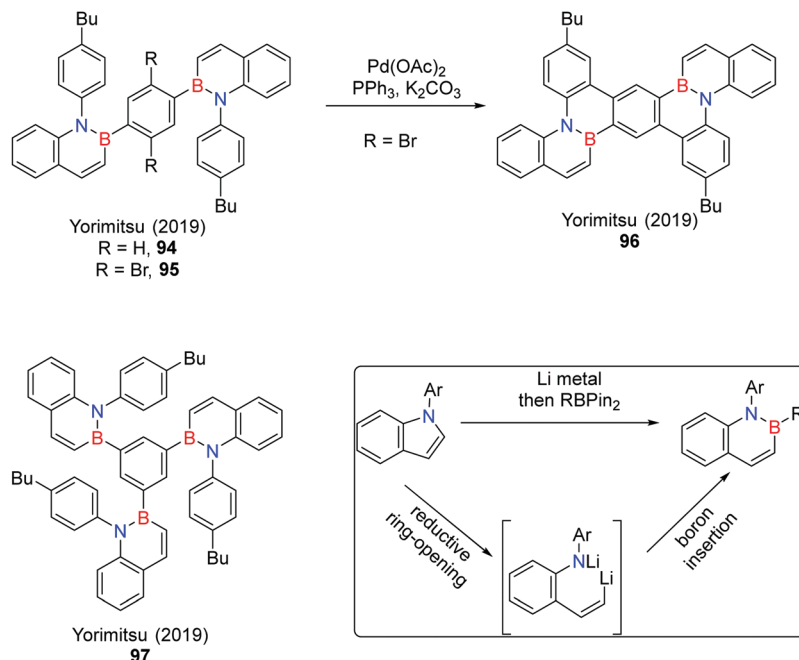


Fig. 28 Synthesis of BN-PAH oligomers via lithium-mediated boron insertion.

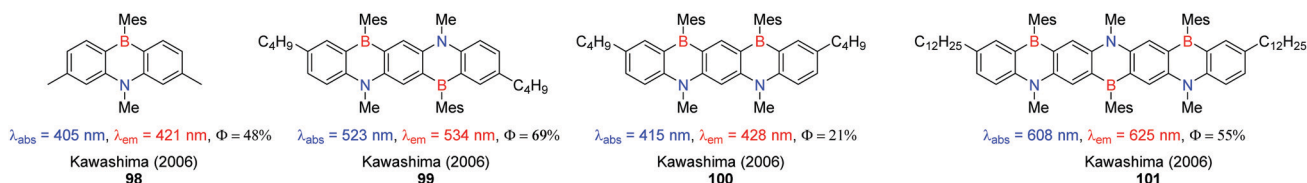


Fig. 29 BN-doped ladder-type acenes with multiple 1,4-BN units.

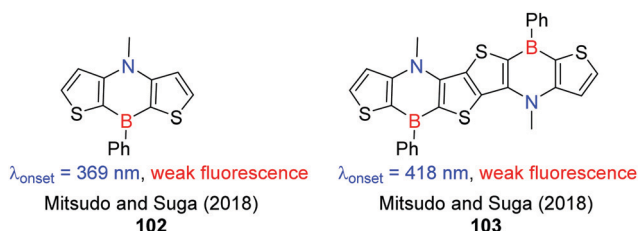


Fig. 30 Dithieno-fused 1,4-azaborine derivatives.

Very recently, Ma and Feng *et al.* reported a modular cascade synthetic strategy to construct structurally constrained BN-PAHs (Fig. 32).<sup>167</sup> The tandem process consisted of three steps: borylative 6-endo-dig cyclization, 1,4-boron migration, and subsequent two-fold electrophilic borylation. This methodology was further verified by the general substrate scope. The bis-BN-doped PAHs **107** and **108** were also obtained by this domino process. The single crystal X-ray diffraction analysis of **107** confirmed the double [4]helicene structure. The solid-state structure of **107** had a  $\pi$ -stacked trimeric sandwich structure with a 2D lamellar  $\pi$ -stacking. The bis-BN-nanographene **101** had red-shifted absorption and emission bands compared with

mono-BN-doped PAH **100**, due to its increased  $\pi$ -conjugation structure. The difference of photophysical properties between anti-parallel bis-BN-nanographene **107** and syn-parallel bis-BN-nanographene **108** is likely due to the opposite orientation of two BN units. All these compounds had very small Stokes shift due to their constrained structures.

### 3.2 1,4-BN-PAHs with MR-TADF

Due to the opposite resonance effect of the boron atoms and nitrogen atoms, the resonance effect could be enhanced by *para*-substitution between the boron atoms and the nitrogen atoms, resulting in substantially separated HOMO and LUMO levels, which is known as multiresonance HOMO–LUMO separation (Fig. 33). In 2016, Hatakeyama and coworkers exploited this strategy to design BN-PAHs DABNA **109** and **110** that exhibited ultrapure blue fluorescence (Fig. 33).<sup>23</sup> Structurally, the introduction of substituents on **110** improved the oscillator strength without changing the localization of molecular orbitals. Both **109** and **110** exhibited excellent quantum yields and small singlet-triplet energy gaps ( $\Delta E_{\text{st}} = 0.20 \text{ eV}$ ). Compared to **109**, the device based on **110** exhibited better electroluminescent performance with an EQE of 20.2%, a current efficiency of 21.1  $\text{cd A}^{-1}$ , a power efficiency of 15.1  $\text{lm W}^{-1}$ ,

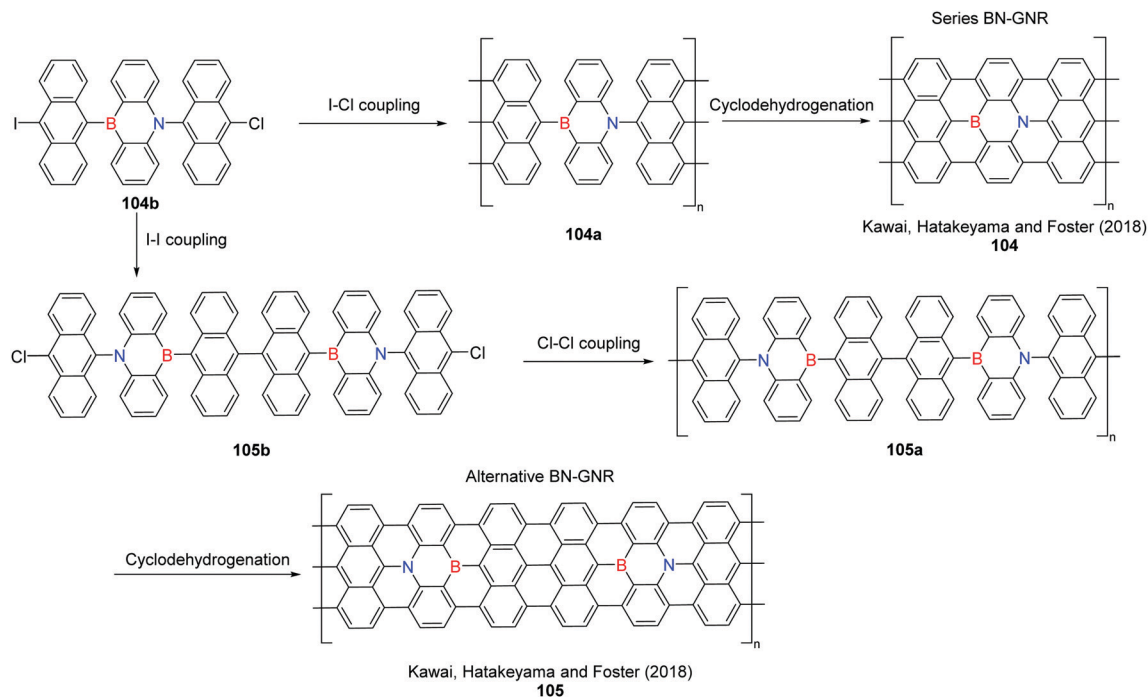


Fig. 31 Multi-BN-doped graphene nanoribbons.

a narrow FWHM of 28 nm and Commission Internationale de l'Eclairage (CIE) coordinates of (0.12, 0.13). The improved performance of **109** might be ascribed to the higher radiative rate ( $k_F = 14.1 \times 10^7 \text{ s}^{-1}$ ) and reverse intersystem crossing decay rate ( $k_{\text{RISC}} = 14.8 \times 10^3 \text{ s}^{-1}$ ). The serious efficiency roll-off was due to the small  $k_{\text{RISC}}$  and charge carrier imbalance. This problem was significantly improved by designing doubled DABNA PAH **111**.<sup>168</sup> The OLED device using **111** as the emitter exhibited narrowband (FWHM = 18 nm) deep-blue emission at 469 nm, indicating that the extended conjugation of PAHs based on multiresonance HOMO–LUMO separation does not result in bathochromic shift of emission. The  $k_F$  and  $k_{\text{RISC}}$  of compound **111** were remarkably increased to  $2.0 \times 10^8 \text{ s}^{-1}$  and  $2.0 \times 10^5 \text{ s}^{-1}$ . The device based on **111** had record-breaking EQEs of 34.4% at the maximum and 26.0% at  $1000 \text{ cd m}^{-2}$ . The bis-BN-PAH **112**, a nitrogen atom replaced with an oxygen atom compared to **111**, showed hypsochromically shifted emission due to oxygen atom incorporation prompted restricted  $\pi$ -conjugation of the HOMO.<sup>169</sup> Further expanded heterohelicene **113** with tripled DABNA was achieved by a one-shot triple borylation.<sup>170</sup> The OLED device based on (BN)<sub>3</sub>-doped helicene **113** showed narrowband red-shifted emission ( $\lambda_{\text{em}} = 480 \text{ nm}$ ) compared to **111**. Although the  $k_{\text{RISC}}$  ( $4.4 \times 10^5 \text{ s}^{-1}$ ) of compound **113** was double that of **111**, the serious efficiency roll-off was still observed probably due to the charge carrier imbalance.

Developing efficient electrophilic borylation reactions plays a critical role in construction of BN-doped PAHs since these reactions are highly dependent on the types of substrates and boron reactants, temperature, and even additives. Hatakeyama *et al.* discovered one-shot multiple borylation using highly Lewis acidic boron reagent  $\text{BI}_3$  to synthesize a series of

BN-nanographenes with different numbers of BN units (Fig. 34).<sup>171</sup> In the presence of 12 eq. of  $\text{BI}_3$ , quadruple borylation reaction was proceeded under reflux conditions affording four-boron atom-doped compound **114** and a small amount of **115**. The tri-BN-doped nanographene **115** was obtained in a much higher yield if less  $\text{BI}_3$  was added in the presence of additive  $\text{Ph}_3\text{B}$  at higher temperature. The same conditions used to access **115** were exploited to achieve bis-BN-doped PAH **116** in a higher yield at relatively lower temperature. The crystal structure of **115** confirmed its helical structure. The absorption maximum (396 nm) of **114** was noteworthy blue-shifted compared to those of **114** (438 nm) and **116** (440 nm) due to the forbidden  $S_0$ – $S_1$  and  $S_0$ – $S_2$  transitions and high oscillator strengths of  $S_0$ – $S_3$  and  $S_0$ – $S_4$ . All these three BN-nanographenes emitted blue fluorescence with moderate to good quantum yields and full-widths at half-maximum (FWHM) between 32 and 38 nm. The phosphorescence maxima of **114**–**116** at 77 K were very close to their fluorescence maxima, indicating that they are promising for TADF-based OLEDs. Compound **116** was selected to demonstrate the potential in OLEDs. The fabricated OLED device showed exceptional performance with a maximum EQE of 18.3%.

The Hatakeyama group and Wang group independently reported the synthesis of BNB-doped PAHs **117** (Fig. 35).<sup>172,173</sup> This class of BNB-doped molecules was found to exhibit efficient MR-TADF, featuring small  $\Delta E_{\text{st}}$ , narrow emission bands (FWHM =  $\sim 33 \text{ nm}$ ), comparable  $k_{\text{RISC}}$  values to that of NBN-doped PAH **109**, and high photoluminescence quantum yields up to 89%. With an extended  $\pi$ -skeleton with oxygen atoms and bulky substituents, compound **118** exhibited solution-processable pure green MR-TADF.<sup>174</sup> Similar to the

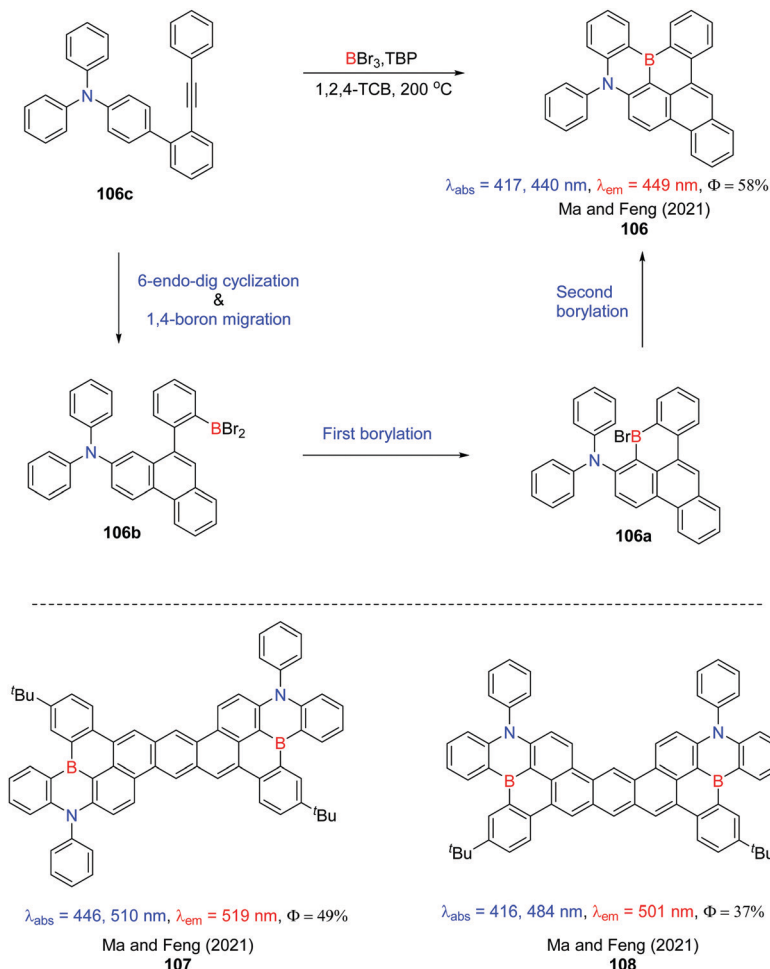


Fig. 32 The cascade synthetic approach toward BN-PAHs.

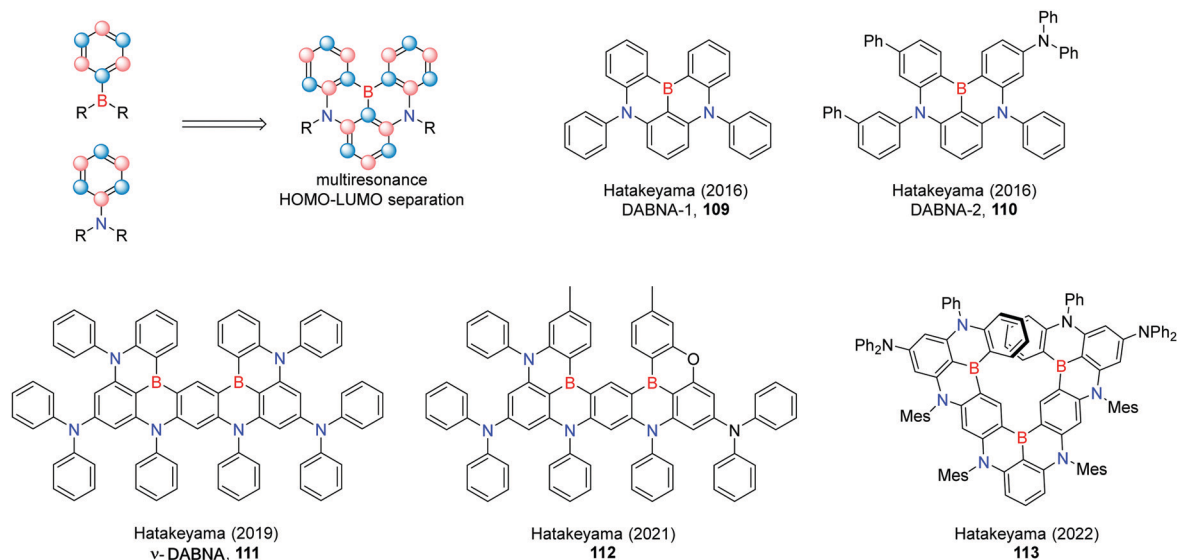


Fig. 33 1,4-BN-PAHs with MR-TADF by Hatakeyama.

other OLED based MR-TADF emitters, the device of **118** presented attractive performances with CIE coordinates of (0.12, 0.63) and EQEs of 21.8% at the maximum and 17.4% at 1000  $\text{cd m}^{-2}$ . The solution-processability of **118** could substantially

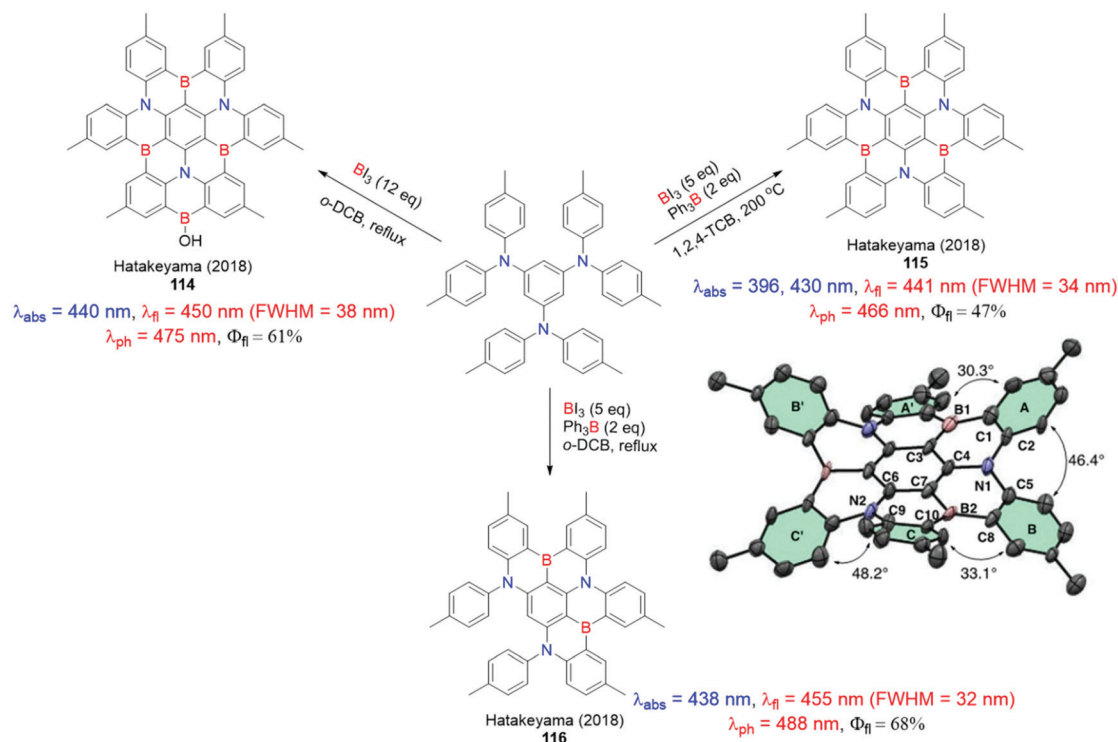


Fig. 34 One-shot multiple borylation toward multi-BN-nanographenes. The crystal structure of **115** reprinted with permission from ref. 171. Copyright 2018 American Chemical Society.

reduce the cost of the device fabrication. Agou and Yasuda *et al.* documented a ternary-doped MR-TADF system (**119**) with multiple boron, nitrogen and sulfur atoms (Fig. 35).<sup>175</sup> In addition to being an electron-rich moiety for inducing the MR effect with the nitrogen atoms, the heavy-atom effect of the phenothiazine moiety has an important impact on enhancing the spin-flipping RISC. The OLED device emitted narrowband sky-blue light with a balance high  $k_{\text{RISC}}$  ( $1.9 \times 10^6 \text{ s}^{-1}$ ) and high  $k_{\text{F}}$  ( $9.0 \times 10^7 \text{ s}^{-1}$ ), a high maximum EQE of 21.0%, and suppressed efficiency roll-off.

Zysman-Colman *et al.* reported a linear ladder-type BN-doped heptacene, **120**, in which three boron atoms were introduced once through electrophilic borylation.<sup>176</sup> Structurally, BN-heptacene **120** is isomeric to compound **121**, which shares the same (BN)<sub>3</sub>-heptacene core with **101**, which was reported by Kawashima and coworkers.<sup>27</sup> Compared to anti-parallelled BN-heptacene **121**, the syn-parallelled BN-heptacene **120** was demonstrated to have higher  $S_1$  energy and deep-blue emission with CIE coordinates of (0.17, 0.01) (Fig. 36). Opposite to **121**, compound **120** exhibited MR-TADF properties at ambient

temperature, which are very rare for linear 1,4-BN-doped PAHs. The distinct difference of singlet and triplet energies as well as the  $\Delta E_{\text{st}}$  once again indicates that the orientation of BN units could significantly impact the optoelectronic properties of BN-PAHs.

As an attractive building block for optoelectronic materials, incorporating the carbazole moiety into BN-doped PAHs has gained more and more attention. Especially, the carbazole-based DABNA **109** analogues have been extensively studied.<sup>177–182</sup> Recently, Hatakeyama *et al.* reported a series of carbazole-based DABNA analogues which have the capability of being highly efficient MR-TADF materials (Fig. 37).<sup>183</sup> The electrophilic borylation has two potential reaction sites: the *ortho* position of the carbazolyl group and the *ortho* position of the diarylamino group. The DFT calculations indicated that the HOMO was mainly localized at the *ortho* position of the carbazolyl group, resulting in compound **122** instead of the compound of borylation at the *ortho* position of the diarylamino group reported by Huang.<sup>177</sup> This showcases that theoretical calculation could be helpful to determine the selectivity of reaction reactive sites.

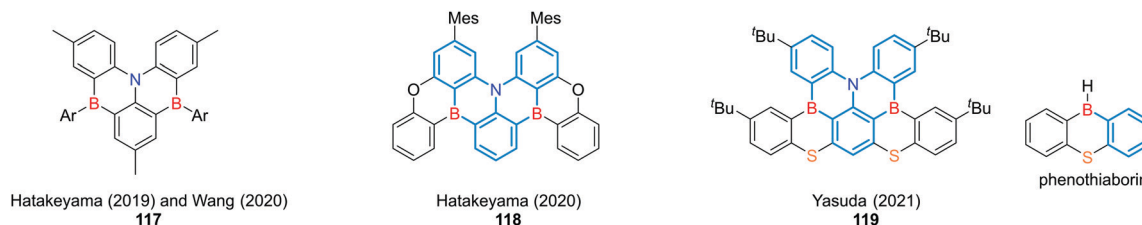
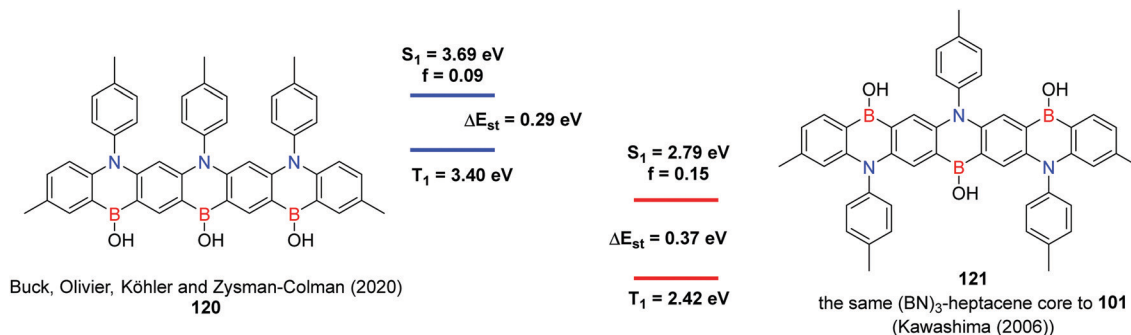


Fig. 35 BNB-doped PAHs for MR-TADF.

Fig. 36 (BN)<sub>3</sub>-doped heptacenes.

All these carbazole-based DABNA molecules had excellent photoluminescence quantum yields with very small  $\Delta E_{ST}$ . Compared to mono-NBN-doped PAHs **122** and **124**, incorporation of the second boron atom red-shifted the emissions and widened the FWHMs of di-NBN-doped PAHs **123** and **125**. The bis-NBN-doped PAH **123** with two *t*-butyl groups replaced with the phenyl group in OLEDs displayed green emission at 497 nm with a FWHM of 29 nm and CIE coordinates (0.12, 0.57).

In order to achieve full-color luminophores, the Yasuda group discovered that strategic implementation of electron-deficient

boron atoms and electron-rich carbazole units provided a variety of BN-PAHs with efficient TADF properties (Fig. 38).<sup>179</sup> The carbazole-based DABNA **126** was independently synthesized and investigated in OLEDs by Duan and Wang.<sup>178,182</sup> The donor strength of the carbazole unit in bis-NBN-doped DABNA analogue **127** was reduced by incorporating the second boron atom at the *para*-position of the carbazole, while the acceptor strength *via* B- $\pi$ -N conjugation was decreased by the fused third carbazole moiety. This resulted in a wider HOMO-LUMO energy gap and blue-shifted emission of **127**. Inversely, the acceptor and donor

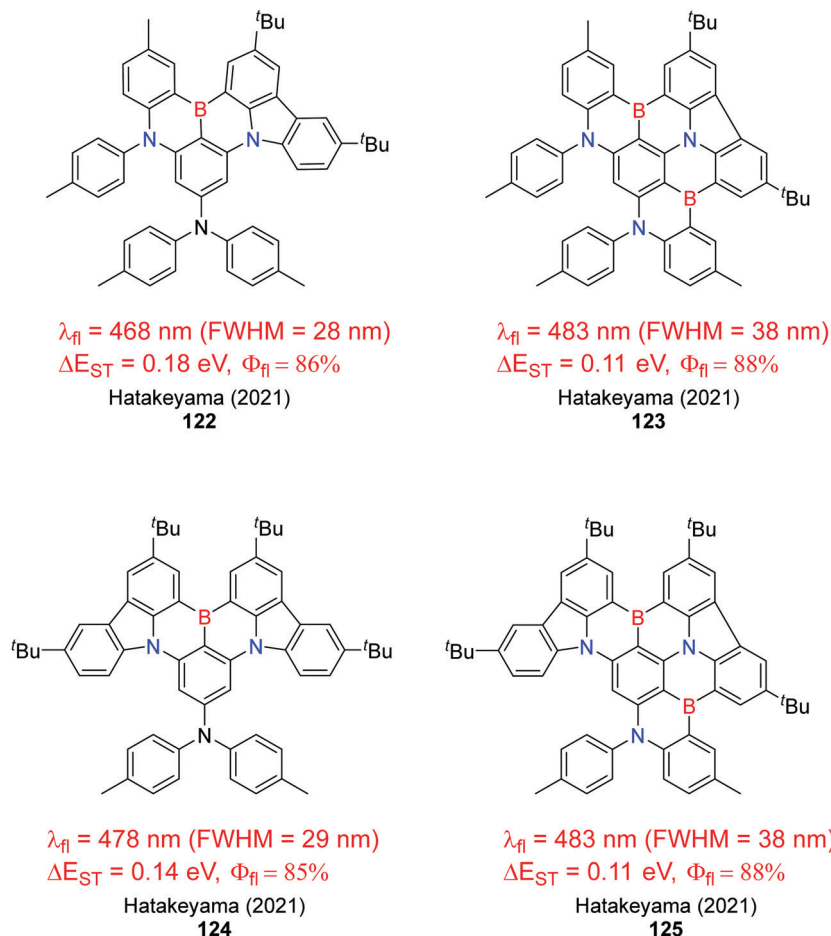


Fig. 37 Carbazole-based multi-BN-doped PAHs developed by Hatakeyama.

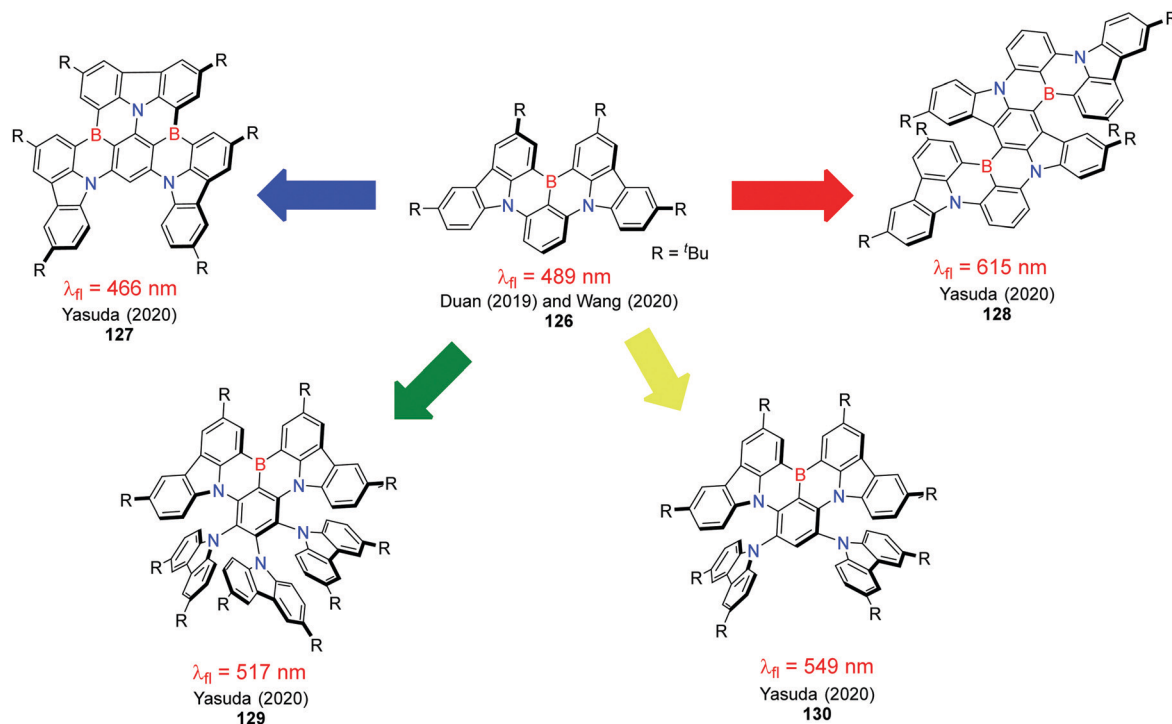
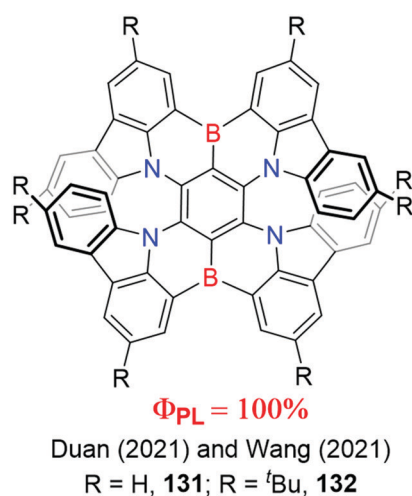


Fig. 38 Carbazole-based multi-BN-doped PAHs with full-color MR-TADF developed by Yasuda.

strengths were substantially increased by the two *para*-doped boron atoms and two nitrogen atoms in **128**, featuring notable bathochromic shifts of the absorption and emission spectra. The HOMOs of **129** and **130** extended to the extra *meta*-positioned carbazoles of the boron atom, which can strengthen the intramolecular charge-transfer (ICT) with lower  $S_1$  and  $T_1$  energies accompanied by red-shifted emissions. Based on the family of MR-TADF PAHs **125–129**, full-color and narrowband OLEDs were obtained with excellent maximum EQEs up to 31.8%.

The fact that non-radiative transitions will dramatically increase with decreasing energy gap, also known as energy gap

law,<sup>184,185</sup> has significantly limited the discovery of deep-red and near-infrared (NIR) emitters with high efficiency. Duan and coworkers reported distorted (NBN)<sub>2</sub>-doped helical molecules **131** and **132** bearing four carbazole units and two boron atoms (Fig. 39).<sup>181</sup> Both **131** and **132** had exceptionally high photoluminescence quantum yields of 100%. The introduction of *t*-butyl groups on carbazole moieties slightly decreased the energy gap with an unchanged FWHM of 38 nm, as well as a significantly slower  $k_{RISC}$ . Not surprisingly, significant efficiency roll-off was observed since the low  $k_{RISC}$  was at the order of  $10^4 \text{ s}^{-1}$ . Almost at the same time, the Wang group independently



#### Application in red OLEDs by Duan

- Deep-red OLEDs
- Record-high maximum EQE of 28%

#### Strong chiroptical response by Wang

- Strong chiroptical activities from 300 to 700 nm
- Record-high  $g_{abs}$  up to 0.033

Fig. 39 Carbazole-based multi-BN-doped helicenes in different applications developed by Wang and Duan. Reprinted with permission from ref. 180. Copyright 2021 American Chemical Society.

demonstrated the same molecules with different application in chiroptical materials.<sup>180</sup> Molecule **131** exhibited a record-high absorption dissymmetry factor ( $g_{\text{abs}}$ ) of up to 0.033 in the visible spectral range and red to near-infrared circularly polarized luminescence (CPL). The HOMO–LUMO separation induced by *para*-positioned boron atoms and nitrogen atoms is related to the high  $g_{\text{abs}}$ .

## 4. Multi-BN-doped $\pi$ -conjugated systems bearing tetracoordinate boron atoms

Multiple BN-doped  $\pi$ -conjugated systems bearing tetracoordinate boron atoms have been extensively studied, especially boron-dipyrromethene (BODIPY) and its derivatives,<sup>186–188</sup> as well as tetracoordinate boron-doped small molecules and polymers and their corresponding applications in OLEDs<sup>189</sup> and OPVs.<sup>190–192</sup> However, we will only focus on two types of PAHs with four-coordinated boron atoms in this section (Fig. 40): (1)  $\pi$ -conjugated systems consisting of 5-membered BN-chelate units and (2)  $\pi$ -conjugated systems consisting of 6-membered BN-chelate units.

### 4.1 $\pi$ -Conjugated systems consisting of 5-membered BN-chelate units

In 2006, Yamaguchi and coworkers exploited the (3-boryl-2-thienyl)-2-thiazole **133** as the building block to design a series of regioisomeric bis-BN-doped  $\pi$ -conjugated systems (Fig. 41).<sup>193</sup> The different orientations of BN units in the dimers **134–136** resulted in blue-shifted absorption and emission bands from **134** ( $\lambda_{\text{abs}} = 443$  nm,  $\lambda_{\text{em}} = 492$  nm) to **136** ( $\lambda_{\text{abs}} = 414$  nm,

$\lambda_{\text{em}} = 472$  nm). Compared to the thienylthiazole backbone, incorporation of BN units not only rendered the  $\pi$ -conjugated framework in a plane, but also lowered the LUMO level. The time-of-flight (TOF) carrier-mobility measurement on a vacuum-deposited film of **134** exhibited a fairly high electron mobility ( $m$ ) of  $1.5 \times 10^{-4}$  cm<sup>2</sup> V<sup>-1</sup> s<sup>-1</sup>.

The N,C-chelate boron compounds was the first class of chelate boron compounds to display reversible photochromism, which was discovered by Wang *et al.* in 2008.<sup>15</sup> The solution of compound **137** could rapidly lose its strong blue fluorescence and change color from colorless to deep blue (Fig. 42) upon irradiation at 365 nm, which could be thermally reversible. Wang and coworkers continued to extend this photochromic N,C-chelate boron systems to dimers **138** linked with a non-conjugated silane and **139** linked with a conjugated 1,4-diethynylbenzene, even oligomer **140** with six N,C-chelate boron units.<sup>194,195</sup> Although these dimers and oligomers of **137** still underwent photochromism, only one boron unit underwent photoisomerization. The photochromism of the remaining boron units in **138–140** was quenched by the intramolecular energy transfer from the non-isomerized boron unit to the dark isomer unit featuring a low energy absorption band.

Intramolecular Lewis acid–base coordination accompanied by the introduction of BN units into ladder-type conjugated molecules usually plays a critical role in the rigid and coplanar structures of these tetracoordinate boron-doped ladder-type molecules as well as the electronic structures. Bis-BN-doped ladder acenes **141–144** with an indacene core with different bilateral units exhibited broad visible to near-infrared (NIR) light absorption (Fig. 43) due to the significantly decreased LUMO level compared to the backbone ligands.<sup>196,197</sup> The surrounding



Fig. 40 Two types of four-coordinated boron-doped PAHs.

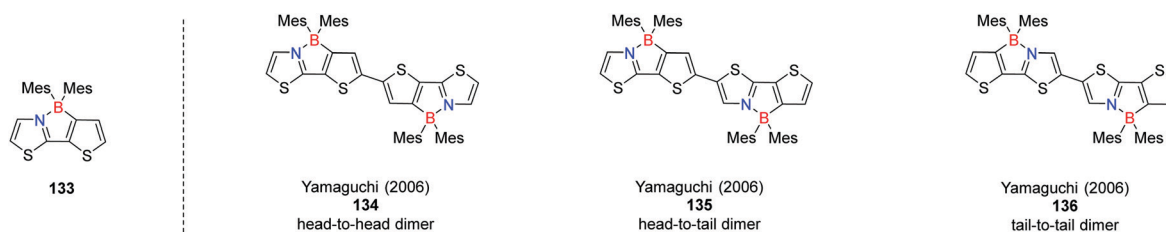


Fig. 41 A series of regioisomeric dimers of 5-membered BN-chelate units by Yamaguchi.



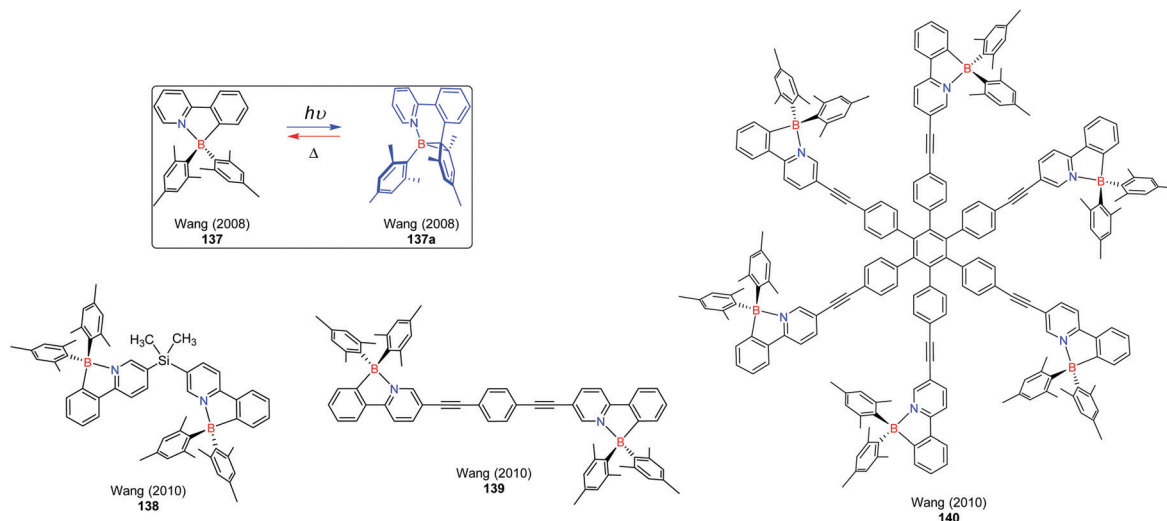


Fig. 42 The multi-BN-doped  $\pi$ -conjugated systems consisting of 5-membered BN-chelate units by Wang.

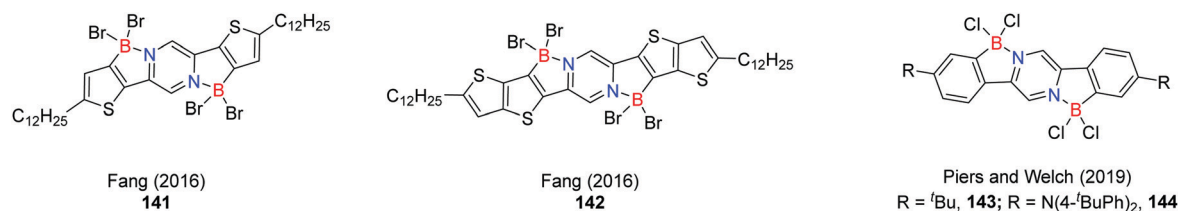


Fig. 43 Bis-BN-doped ladder acenes with an indacene core.

substituents were found to have an essential impact on the absorption maxima of **143** ( $R = {}^t\text{Bu}$ ) and **144** ( $R = \text{N}(4\text{-}{}^t\text{BuPh})_2$ ). Replacing the halide substituents on boron atoms with aromatic substituents (e.g. tolyl, 2,4,6- $\text{F}_3\text{C}_6\text{H}_2$ ) of **143** and **144** resulted in lower energy absorption significantly blue-shifted. Using compound **143** with Cl replaced with 2,4,6- $\text{F}_3\text{C}_6\text{H}_2$ , proof-of concept organic solar cells (OSCs) were fabricated with power conversion efficiencies of 2%.

A series of bis-BN-doped ladder-type pyrrolo[3,2-*b*]pyrroles were synthesized, featuring large molar extinction coefficients and orange to deep red fluorescence with quantum yields up to

90% (Fig. 44).<sup>198</sup> These dyes exhibited superb photostability and high post-functionalization capability; a variety of R groups in compounds **145** and **146** were introduced with tunable photophysical properties. Large two-photon absorption cross sections were observed in these dyes.

The introduction of BN units could not only induce unique photophysical properties and intermolecular interactions, but also make the synthesis of BN-doped molecules simpler compared to the synthesis of their all-carbon analogues because a B–N dative bond usually can be much more easily formed than a C–C bond. For example, carbon-bridged oligophenylenevinylenes

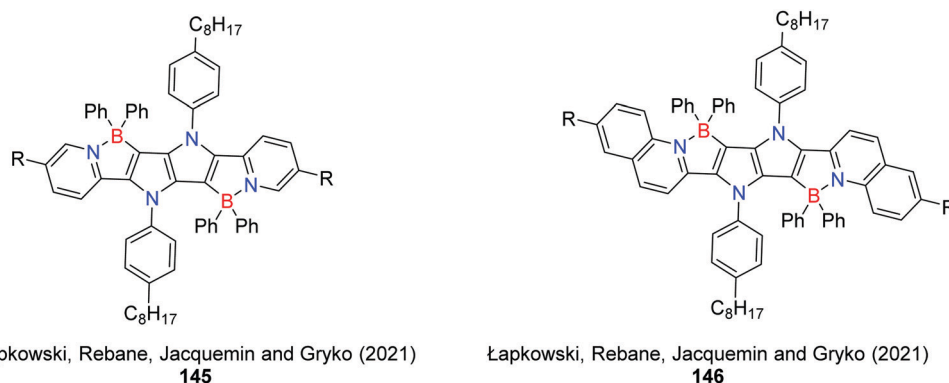


Fig. 44 Bis-BN-doped ladder acenes fused with pyrrolo[3,2-*b*]pyrrole.

((COPV)<sub>n</sub>, **147**) have been used in molecular wire and solid-state lasers; however, the synthesis of COPV oligomers with long wavelengths of emission is very challenging.<sup>199–201</sup> Replacing the CC unit with the BN unit could result in feasible synthesis and longer wavelengths of emission. Recently, Shang, Nakamura and coworkers reported a class of linear bis-BN-doped  $\pi$ -conjugated molecules through four-step synthesis in high yields (Fig. 45).<sup>202</sup> The absorption and emission bands of **148** were red-shifted about 40–50 nm compared to its carbonaceous analogue ((COPV)<sub>2</sub>, **147**). The extension of  $\pi$ -conjugation in **149** further moved the absorption and emission spectra toward the long wavelength direction. Incorporation of BN units still kept the structures as rigid as the all-carbon analogue, so the quantum yields of the bis-BN-doped ladder-type molecules **148** and **149** were close to unity, which was similar to that of (COPV)<sub>2</sub>. The LUMO levels of **148** and **149** were significantly decreased compared to (COPV)<sub>2</sub>, while the HOMO levels of **148** and **149** remained almost unchanged. COPVs and their two BN-doped congeners **148** and **149** showed similarly high photostability. The molecules **148** and **149** served as lipophilic fluorescent dyes for live cell imaging with unchanged sky-blue and yellow fluorescence in 25 min under irradiation, respectively, which is superior to commercially available BODIPY-based dyes.

Recently, helicenes have attracted increasing attention as chiroptical dyes due to their enhanced circular dichroism (CD) and circularly polarized luminescence (CPL) properties compared with other chiral organic molecules.<sup>203,204</sup> However, helicenes usually show low fluorescence quantum yields due to the low transition probability of the first excited state S<sub>1</sub>.<sup>205,206</sup> Introducing boron atoms into helicenes has proven to be an effective way for increasing quantum yields.<sup>145,180</sup> Nowak-Król *et al.* discovered a modular synthesis of mono-BN-doped azabora[7]helicenes **150** and bis-BN-doped

azabora[9]helicenes **151** *via* an electrophilic borylation followed by a substitution reaction with aluminum reagents (Fig. 46).<sup>207</sup> In contrast to the high configurational stability of **150**, the bis-BN-doped helicenes **151** showed the interconversion of four conformers *via* three transition states. The interconversion of **151** was observed at room temperature, which made the resolution of the stereoisomers impossible. Azabora[7]helicenes **150** exhibited strong chiroptical response with large dissymmetry factors of up to  $1.12 \times 10^{-2}$  and noteworthy higher fluorescence quantum yields of 18–24% than those of [6]carbohelicenes. The azabora[9]helicenes **151** showed brighter emission with quantum yields of 43–47%.

#### 4.2 $\pi$ -Conjugated systems consisting of 6-membered BN-chelate units

Doping four-coordinated boron atoms into  $\pi$ -conjugated systems could markedly decrease the LUMO level and increase the electron affinity, which is also true for  $\pi$ -conjugated systems consisting of 6-membered BN-chelate units.<sup>192,208,209</sup> In the subsection, we will focus on molecules with exceptionally low LUMO levels in different applications.

In addition to the lowered LUMO level, the introduction of BN units could also endow tetracoordinate boron-doped  $\pi$ -conjugated systems with remarkable redox activities. Fang and coworkers designed two cruciform ladder-type molecules **152** and **153** (Fig. 47) with the B  $\leftarrow$  N coordination-promoted delocalization and hyperconjugation.<sup>210</sup> These two molecules featured two reversible oxidation peaks and two reversible reduction peaks, corresponding to five stable redox states, as shown at the bottom of Fig. 47. The gain of electrons and loss of electrons of compound **153** were accompanied by the interconversion of different forms of its central core between a

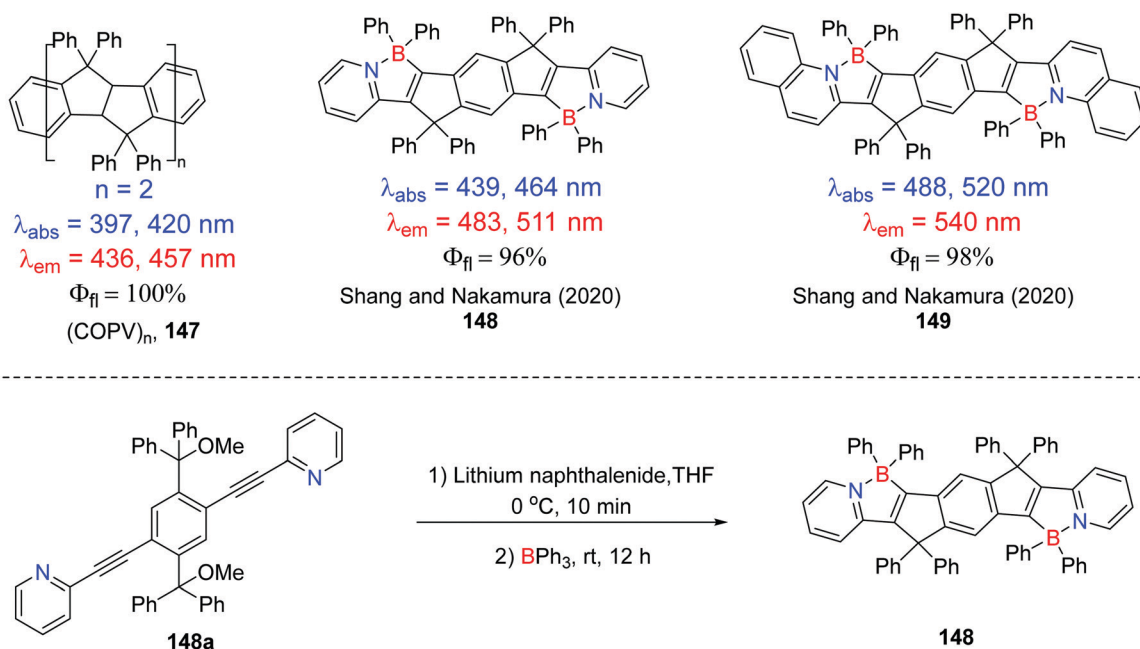


Fig. 45 Bis-BN-(COPV)<sub>2</sub>.

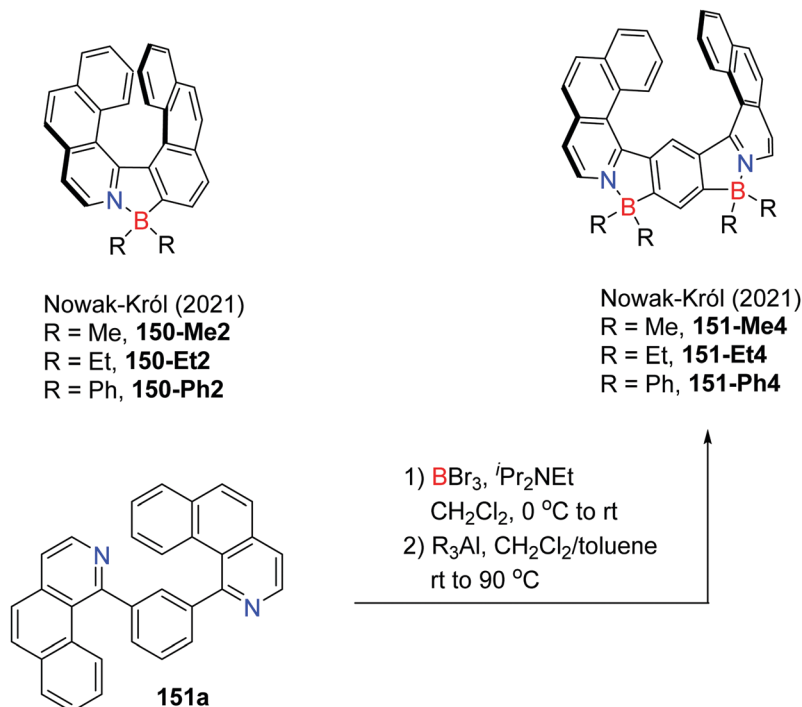
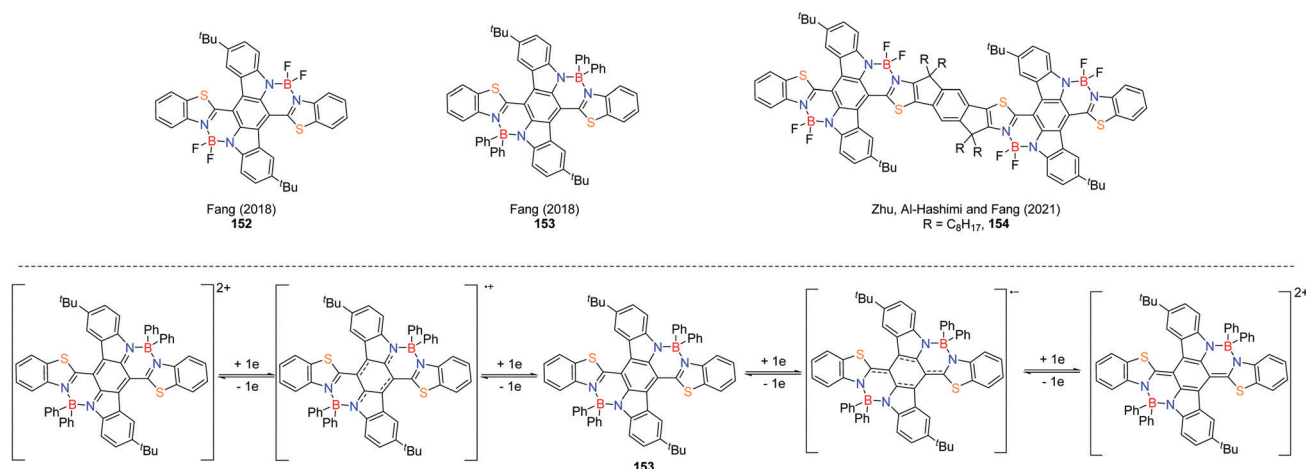


Fig. 46 Bis-BN-doped organoboron helicenes.

benzenoid character and two quinonoid characters. Both **152** and **153** showed reversible multicolor electrochromism. The molecule **153** with phenyl groups on the boron atoms displayed red-shifted absorption and emission bands ( $\lambda_{\text{abs}} = 768\text{ nm}$ ,  $\lambda_{\text{em}} = 812\text{ nm}$ ) compared to that of **152** with fluoride on the boron atoms ( $\lambda_{\text{abs}} = 695\text{ nm}$ ,  $\lambda_{\text{em}} = 720\text{ nm}$ ). Low fluorescence quantum yields of **152** ( $\Phi_{\text{fl}} = 2.8\%$ ) and **153** ( $\Phi_{\text{fl}} = 1.2\%$ ) were measured due to their small energy band gaps. Very recently, collaborating with Zhu and Al-Hashimi, Fang and coworkers documented a quadruply BN-doped polycyclic  $\pi$ -system with 23 fused rings (**154** in Fig. 47).<sup>211</sup> This large ladder-type molecule **154** exhibited intensive absorption in the NIR region with a decreased LUMO level of  $-3.82\text{ eV}$ .

Liu and coworkers reported a tetracoordinate boron-doped pyrene with two strong electron-withdrawing groups (Fig. 48a).<sup>212</sup> Due to the delocalized LUMO at  $-3.93\text{ eV}$  spread over the entire molecule and the localized HOMO at the BN-pyrene core, compound **155** exhibited a wide absorption spectrum in the visible range with two absorption maxima at  $\lambda_{\text{max}} = 502\text{ nm}$  and  $771\text{ nm}$ . OSCs based on **155** were reported to have a power conversion efficiency of 7.06%. A similar doping strategy has been used in the synthesis of tri-NBN-doped triazatrinaphthylene (Fig. 48b).<sup>213</sup> Both **156** and **157** exhibited a disc-shaped and slightly deformed skeleton. The molecule **157** with phenyl groups on the boron atoms showed *ca.* 30 nm red-shift in absorption and *ca.* 80 nm red-shift in emission compared to compound **156** with fluorides

Fig. 47 Multi-BN-doped ladder-type conjugated molecules based on the indolo[3,2-*b*]carbazole.

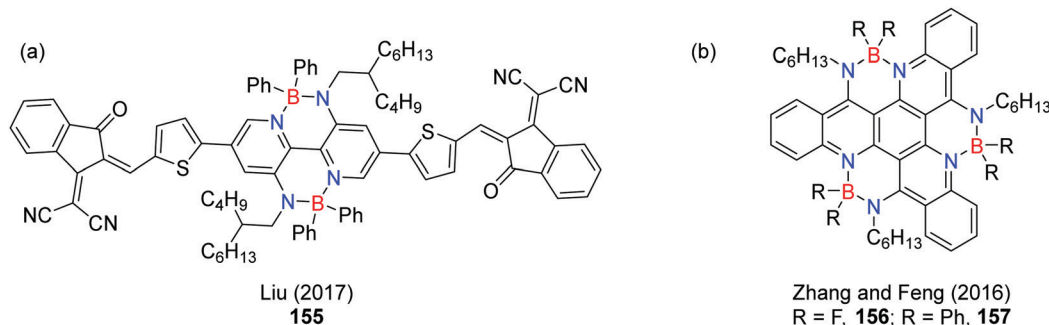


Fig. 48 (a) Doubly NBN-doped pyrene and (b) triply NBN-doped triazatrinaphthylene with tetracoordinate boron atoms.

on the boron atoms. The low quantum yields of **156** ( $\Phi_{\text{fl}} = 2.46\%$ ) and **157** ( $\Phi_{\text{fl}} = 1.91\%$ ) were probably due to the deformed structure-enhanced nonradiative decay. The substituents on the boron atoms have been found to have a substantial impact on the electrochemical behaviors.

Liu and coworkers systematically investigated how B ← N coordination affects the optoelectronic properties and device behaviors (Fig. 49).<sup>24–26</sup> When two NBN units were doped into the same conjugated system, the different locations of NBN units had notable effects on the frontier molecular orbitals, particularly on the LUMO level. The 1,4-NBN-positioned molecule **160** had the lowest LUMO up to  $-4.01$  eV among molecules **158–160**. The molecule **160** and 1,2-NBN-positioned molecule **158** showed electron transporting properties with mobilities of  $0.06$  and  $0.12$   $\text{cm}^2 \text{V}^{-1} \text{s}^{-1}$ , respectively. The 1,3-NBN-doped molecule **159** had the highest LUMO among these three molecules with ambipolar electron/hole transporting behaviors ( $\mu_{\text{h}} = 4.2 \times 10^{-3} \text{cm}^2 \text{V}^{-1} \text{s}^{-1}$ ,  $\mu_{\text{e}} = 0.07 \text{cm}^2 \text{V}^{-1} \text{s}^{-1}$ ). Compounds **158** and **159** showed strong absorption spectra with maxima near  $700$  nm and emitted NIR fluorescence, while the regioisomer **160** exhibited further red-shifted absorption at  $\lambda_{\text{max}} = 808$  nm and emitted no fluorescence. These differences in optoelectronic properties again indicate that the location and orientation of BN units should be fully taken into account. The PAHs **161–163** with four NBN units further lowered the LUMO levels. The disc-type molecule **161** displayed a well-resolved absorption spectrum with two major peaks at  $569$

and  $618$  nm, as well as an intense NIR fluorescence spectrum with a small Stokes shift and an exceptional quantum yield of up to  $50\%$ . Compared to compound **162**, the molecule **163** with two extra bilateral benzo rings exhibited the lowest LUMO level of up to  $-4.58$  eV among boron-doped  $\pi$ -conjugated molecules. Compared to the average electron mobilities less than  $10^{-2} \text{cm}^2 \text{V}^{-1} \text{s}^{-1}$ , the electron mobility of **163** in OFETs was two orders of magnitude higher up to  $1.60 \text{cm}^2 \text{V}^{-1} \text{s}^{-1}$ . This indicates that pushing the number limit of BN units in PAHs could help achieve certain properties that could not be accessed by other types of molecules.

The introduction of tetracoordinate boron into conjugated molecules can not only lead to functional materials with properties mentioned above like photochromism, NIR-absorption/emission, and significantly lowered LUMO levels, but also enhance the singlet  $\text{O}_2$  sensitivity. In 2017, Jäkle *et al.* reported a class of tetra-coordinated boron-functionalized anthracenes (Fig. 50).<sup>214</sup> Compared to the all-carbon analogues, the doubly BN-fused anthracenes **164** and **165** showed dramatically decreased LUMO levels with slightly increased HOMO levels. The intensively red colored compounds **164** and **165** were found to rapidly react with oxygen upon photoirradiation with the formation of colorless endoperoxides **164** +  $\text{O}_2$  and **165** +  $\text{O}_2$ , respectively. Unlike the reactions of other diarylanthracenes with oxygen which usually require an external photosensitizer, the BN-functionalized anthracenes **164** and **165** underwent the  $\text{O}_2$  sensitization through a self-sensitizing process. This  $\text{O}_2$

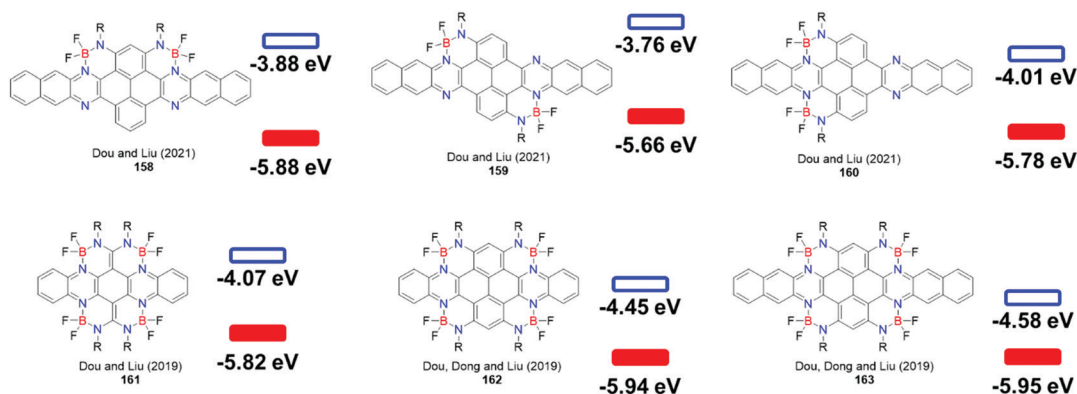


Fig. 49 Multiple NBN-doped PAHs with low LUMO levels and high electron affinity.

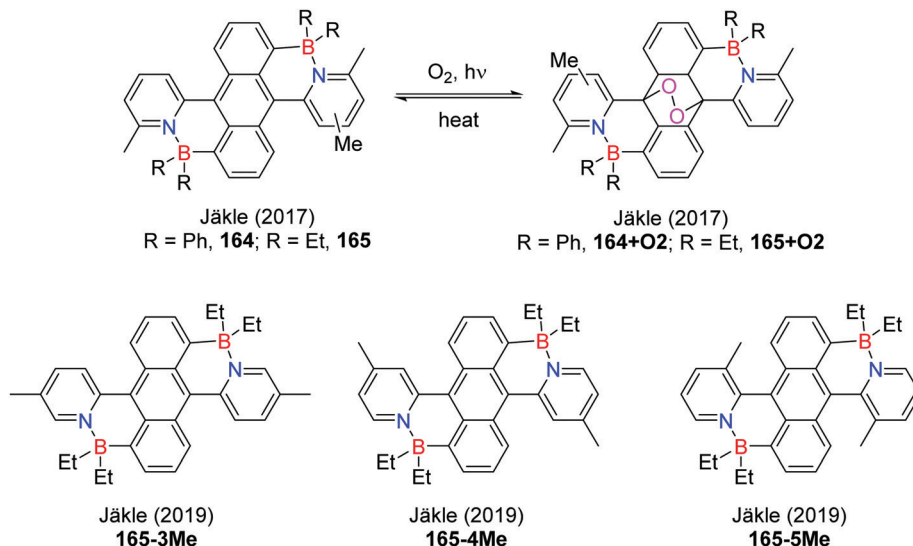


Fig. 50 Doubly BN-fused anthracenes for singlet O<sub>2</sub> sensitization.

sensitization process could be thermally reversed back. The high reactivity of **164** and **165** toward O<sub>2</sub> was mainly ascribed to the strong absorption in the visible range, small  $\Delta E_{\text{st}}$ , and the release of steric strain. Further studies indicated that the position of methyl groups on pyridyl rings sterically and electronically affected the self-sensitized reactivity with singlet O<sub>2</sub>. Compounds **165**, **165-3Me**, **165-4Me** and **165-5Me** showed different reaction rates toward O<sub>2</sub> sensitization as well as the thermal release reaction of O<sub>2</sub>.<sup>215</sup>

The introduction of BN units at the zigzag edges of PAHs is regarded as an effective strategy to improve their chemical stabilities. This is particularly useful to stabilize large acenes (longer than pentacene) which are usually unstable in the carbonaceous form. Recently, Ma, Liu and Feng *et al.* documented the synthesis of a class of BN-doped large acenes (Fig. 51).<sup>216</sup> All the modified acenes exhibited high stability. Unlike previous examples in which the BN units affect the LUMO level, the bis-BN-doped acenes **167**–**169** showed higher HOMO levels than the mono-BN-doped PAH **166** with nearly unchanged LUMO levels. The fusing units in compounds **167**–**169** also had a notable impact on the HOMO level; that is, the larger the fusing unit is, the higher HOMO level the BN-doped acene has. With respect to emission, the emission maxima moved toward the long wavelength following the order of **166**, **167**, and **168**. The quantum yields decreased by following the same trend. The pyrene-fused acene **169** was non-emissive due

to the forbidden transition from the lowest-lying excited state to the ground state.

## 5. Conclusions and outlook

In this Review, we have summarized the major contributions to recent progress in the synthesis of multi-BN doped  $\pi$ -conjugated systems as well as their optoelectronic properties. The influence of the location, number and orientation of BN dopants as well as the boron coordination number on structures and optoelectronic properties has been compared if applicable.

Although 1,2-BN-doped PAHs consist of the largest multi-BN-doped  $\pi$ -conjugated systems, only a few of them have been used in optoelectronic devices like OFETs. Therefore, in addition to constructing novel structures, searching for new applications of 1,2-BN-doped PAHs is highly demanded, especially with the aid of a molecular engineering strategy to modify the existing molecules. 1,4-BN-doped PAHs have exhibited promising in OLEDs; however, the roll-off problem of OLEDs based on 1,4-BN-doped PAHs with MR-TADF has limited their practical applications. Tetracoordinate boron-doped PAHs have showed many different applications like photochromism, OFETs and O<sub>2</sub> sensitization, but the PAHs with the four-coordinated boron atoms doped into the center of PAHs rather

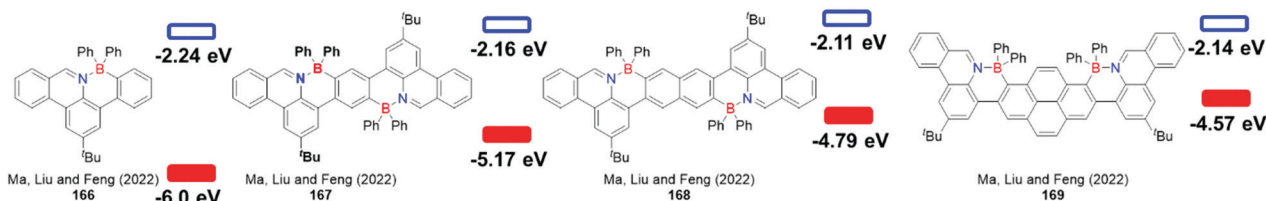


Fig. 51 Large acene derivatives doped with two BN units.

than edges are still quite limited. Certainly, developing new methodologies for introducing boron atoms into  $\pi$ -conjugated systems is fundamentally important.

At last, as the models for studying defected graphene,  $\pi$ -conjugated systems containing heptagonal rings have attracted increasing attention due to their dynamic behaviors, electronic properties, aromaticity and solid-state packing. Doping heptagon-containing  $\pi$ -conjugated systems with the BN unit not only makes  $\pi$ -conjugated systems with the boron-doped heptagonal ring have structural similarity to their all-carbon analogues, but could also significantly change their electronic properties and intermolecular interactions.

## Conflicts of interest

There are no conflicts to declare.

## Acknowledgements

The authors thank the National Natural Science Foundation of China (22001211) and Northwestern Polytechnical University for financial support. This project is also supported by the Fundamental Research Funds for the Central Universities.

## References

- B. Geffroy, P. le Roy and C. Prat, *Polym. Int.*, 2006, **55**, 572–582.
- H.-W. Chen, J.-H. Lee, B.-Y. Lin, S. Chen and S.-T. Wu, *Light Sci. Appl.*, 2018, **7**, 17168.
- P. M. Beaujuge and J. M. J. Fréchet, *J. Am. Chem. Soc.*, 2011, **133**, 20009–20029.
- P. Cheng, G. Li, X. Zhan and Y. Yang, *Nat. Photon.*, 2018, **12**, 131–142.
- W. Wu, Y. Liu and D. Zhu, *Chem. Soc. Rev.*, 2010, **39**, 1489–1502.
- C. Wang, H. Dong, W. Hu, Y. Liu and D. Zhu, *Chem. Rev.*, 2012, **112**, 2208–2267.
- H. Sirringhaus, *Adv. Mater.*, 2014, **26**, 1319–1335.
- Y. S. Zhao, H. Fu, A. Peng, Y. Ma, D. Xiao and J. Yao, *Adv. Mater.*, 2008, **20**, 2859–2876.
- J.-D. Zhou, W.-Q. Zhang, L.-L. Liu, Z.-Q. Xie and Y.-G. Ma, *Chinese Chem. Lett.*, 2016, **27**, 1350–1356.
- S. Revoju, A. Matuhina, L. Canil, H. Salonen, A. Hiltunen, A. Abate and P. Vivo, *J. Mater. Chem. C*, 2020, **8**, 15486–15506.
- W. Jiang, Y. Li and Z. Wang, *Chem. Soc. Rev.*, 2013, **42**, 6113–6127.
- G. Biagiotti, I. Perini, B. Richichi and S. Cicchi, *Molecules*, 2021, **26**, 6306.
- C. Dou, S. Saito, K. Matsuo, I. Hisaki and S. Yamaguchi, *Angew. Chem., Int. Ed.*, 2012, **51**, 12206–12210.
- S. Saito, K. Matsuo and S. Yamaguchi, *J. Am. Chem. Soc.*, 2012, **134**, 9130–9133.
- Y.-L. Rao, H. Amarne, S.-B. Zhao, T. M. McCormick, S. Martić, Y. Sun, R.-Y. Wang and S. Wang, *J. Am. Chem. Soc.*, 2008, **130**, 12898–12900.
- P. G. Campbell, A. J. V. Marwitz and S.-Y. Liu, *Angew. Chem., Int. Ed.*, 2012, **51**, 6074–6092.
- C. R. McConnell and S.-Y. Liu, *Chem. Soc. Rev.*, 2019, **48**, 3436–3453.
- X.-Y. Wang, J.-Y. Wang and J. Pei, *Chem. – Eur. J.*, 2015, **21**, 3528–3539.
- J. Huang and Y. Li, *Front. Chem.*, 2018, **6**, 341.
- X.-Y. Wang, H.-R. Lin, T. Lei, D.-C. Yang, F.-D. Zhuang, J.-Y. Wang, S.-C. Yuan and J. Pei, *Angew. Chem., Int. Ed.*, 2013, **52**, 3117–3120.
- X.-Y. Wang, F.-D. Zhuang, R.-B. Wang, X.-C. Wang, X.-Y. Cao, J.-Y. Wang and J. Pei, *J. Am. Chem. Soc.*, 2014, **136**, 3764–3767.
- X.-Y. Wang, F.-D. Zhuang, X. Zhou, D.-C. Yang, J.-Y. Wang and J. Pei, *J. Mater. Chem. C*, 2014, **2**, 8152–8161.
- T. Hatakeyama, K. Shiren, K. Nakajima, S. Nomura, S. Nakatsuka, K. Kinoshita, J. Ni, Y. Ono and T. Ikuta, *Adv. Mater.*, 2016, **28**, 2777–2781.
- Y. Min, C. Dou, D. Liu, H. Dong and J. Liu, *J. Am. Chem. Soc.*, 2019, **141**, 17015–17021.
- Y. Min, C. Dou, H. Tian, J. Liu and L. Wang, *Chem. Commun.*, 2019, **55**, 3638–3641.
- Y. Min, C. Dou, H. Tian, J. Liu and L. Wang, *Chem. – Eur. J.*, 2021, **27**, 4364–4372.
- T. Agou, J. Kobayashi and T. Kawashima, *Org. Lett.*, 2006, **8**, 2241–2244.
- A. N. Brown, B. Li and S.-Y. Liu, *J. Am. Chem. Soc.*, 2015, **137**, 8932–8935.
- X.-Y. Wang, A. Narita, X. Feng and K. Müllen, *J. Am. Chem. Soc.*, 2015, **137**, 7668–7671.
- Z. Liu, J. S. A. Ishibashi, C. Darrigan, A. Dargelos, A. Chrostowska, B. Li, M. Vasiliu, D. A. Dixon and S.-Y. Liu, *J. Am. Chem. Soc.*, 2017, **139**, 6082–6085.
- Q. Zhang, Z. Sun, L. Zhang, M. Li, L. Zi, Z. Liu, B. Zhen, W. Sun and X. Liu, *J. Org. Lett.*, 2020, **85**, 7877–7883.
- P.-F. Zhang, J.-C. Zeng, F.-D. Zhuang, K.-X. Zhao, Z.-H. Sun, Z.-F. Yao, Y. Lu, X.-Y. Wang, J.-Y. Wang and J. Pei, *Angew. Chem., Int. Ed.*, 2021, **60**, 23313–23319.
- M. Stępień, E. Gońka, M. Żyła and N. Sprutta, *Chem. Rev.*, 2017, **117**, 3479–3716.
- M. Hirai, N. Tanaka, M. Sakai and S. Yamaguchi, *Chem. Rev.*, 2019, **119**, 8291–8331.
- K. Dhbaibi, L. Favereau and J. Crassous, *Chem. Rev.*, 2019, **119**, 8846–8953.
- A. Borissov, Y. K. Maurya, L. Moshniaha, W.-S. Wong, M. Żyła-Karwowska and M. Stępień, *Chem. Rev.*, 2022, **122**, 565–788.
- B. N. Boden, K. J. Jardine, A. C. W. Leung and M. J. MacLachlan, *Org. Lett.*, 2006, **8**, 1855–1858.
- J.-Y. Li, H.-I. Chang, C.-N. Feng and Y.-T. Wu, *Org. Lett.*, 2016, **18**, 6444–6447.
- J. Kaleta and C. Mazal, *Org. Lett.*, 2011, **13**, 1326–1329.
- K. Bera, S. Sarkar, S. Jalal and U. Jana, *J. Org. Lett.*, 2012, **77**, 8780–8786.
- A. Kovács, A. Vasas and J. Hohmann, *Phytochemistry*, 2008, **69**, 1084–1110.

- 42 M. J. S. Dewar, V. P. Kubba and R. Pettit, *J. Chem. Soc.*, 1958, 3073–3076, DOI: [10.1039/JR9580003073](https://doi.org/10.1039/JR9580003073).
- 43 M. J. S. Dewar, C. Kaneko and M. K. Bhattacharjee, *J. Am. Chem. Soc.*, 1962, **84**, 4884–4887.
- 44 A. Abengózar, P. García-García, D. Sucunza, L. M. Frutos, O. Castaño, D. Sampedro, A. Pérez-Redondo and J. J. Vaquero, *Org. Lett.*, 2017, **19**, 3458–3461.
- 45 A. Abengózar, M. A. Fernández-González, D. Sucunza, L. M. Frutos, A. Salgado, P. García-García and J. J. Vaquero, *Org. Lett.*, 2018, **20**, 4902–4906.
- 46 A. Abengózar, P. García-García, D. Sucunza, D. Sampedro, A. Pérez-Redondo and J. J. Vaquero, *Org. Lett.*, 2019, **21**, 2550–2554.
- 47 A. Abengózar, D. Sucunza, P. García-García, D. Sampedro, A. Pérez-Redondo and J. J. Vaquero, *J. Org. Lett.*, 2019, **84**, 7113–7122.
- 48 M. J. D. Bosdet, C. A. Jaska, W. E. Piers, T. S. Sorensen and M. Parvez, *Org. Lett.*, 2007, **9**, 1395–1398.
- 49 J.-S. Lu, S.-B. Ko, N. R. Walters, Y. Kang, F. Sauriol and S. Wang, *Angew. Chem., Int. Ed.*, 2013, **52**, 4544–4548.
- 50 C. Zhang, L. Zhang, C. Sun, W. Sun and X. Liu, *Org. Lett.*, 2019, **21**, 3476–3480.
- 51 L. Zi, J. Zhang, C. Li, Y. Qu, B. Zhen, X. Liu and L. Zhang, *Org. Lett.*, 2020, **22**, 1499–1503.
- 52 S. S. Chissick, M. J. S. Dewar and P. M. Maitlis, *Tetrahedron Lett.*, 1960, **1**, 8–10.
- 53 J. S. A. Ishibashi, J. L. Marshall, A. Mazière, G. J. Lovinger, B. Li, L. N. Zakharov, A. Dargelos, A. Graciaa, A. Chrostowska and S.-Y. Liu, *J. Am. Chem. Soc.*, 2014, **136**, 15414–15421.
- 54 O. Ouadoudi, T. Kaehler, M. Bolte, H.-W. Lerner and M. Wagner, *Chem. Sci.*, 2021, **12**, 5898–5909.
- 55 W. Li, C.-Z. Du, X.-Y. Chen, L. Fu, R.-R. Gao, Z.-F. Yao, J.-Y. Wang, W. Hu, J. Pei and X.-Y. Wang, *Angew. Chem., Int. Ed.*, 2022, e202201464.
- 56 M. J. S. Dewar and W. H. Poesche, *J. Org. Lett.*, 1964, **29**, 1757–1762.
- 57 M. J. D. Bosdet, W. E. Piers, T. S. Sorensen and M. Parvez, *Angew. Chem., Int. Ed.*, 2007, **46**, 4940–4943.
- 58 S. Wang, D.-T. Yang, J. Lu, H. Shimogawa, S. Gong, X. Wang, S. K. Mellerup, A. Wakamiya, Y.-L. Chang, C. Yang and Z.-H. Lu, *Angew. Chem., Int. Ed.*, 2015, **54**, 15074–15078.
- 59 S. Wang, D. T. Yang, J. Lu, H. Shimogawa, S. Gong, X. Wang, S. K. Mellerup, A. Wakamiya, Y. L. Chang, C. Yang and Z. H. Lu, *Angew. Chem., Int. Ed.*, 2015, **54**, 15074–15078.
- 60 S. Mathew, N. A. Astani, B. F. E. Curchod, J. H. Delcamp, M. Marszalek, J. Frey, U. Rothlisberger, M. K. Nazeeruddin and M. Grätzel, *J. Mater. Chem. A*, 2016, **4**, 2332–2339.
- 61 H. Qiao, Y. Deng, R. Peng, G. Wang, J. Yuan and S. Tan, *RSC Adv.*, 2016, **6**, 70046–70055.
- 62 J. Feng, Y. Jiao, W. Ma, M. K. Nazeeruddin, M. Grätzel and S. Meng, *J. Phys. Chem. C*, 2013, **117**, 3772–3778.
- 63 J. H. Delcamp, A. Yella, T. W. Holcombe, M. K. Nazeeruddin and M. Grätzel, *Angew. Chem., Int. Ed.*, 2013, **52**, 376–380.
- 64 C. Li, Y. Liu, Z. Sun, J. Zhang, M. Liu, C. Zhang, Q. Zhang, H. Wang and X. Liu, *Org. Lett.*, 2018, **20**, 2806–2810.
- 65 T. Kaehler, M. Bolte, H.-W. Lerner and M. Wagner, *Angew. Chem., Int. Ed.*, 2019, **58**, 11379–11384.
- 66 S. Kumagai, H. Ishii, G. Watanabe, C. P. Yu, S. Watanabe, J. Takeya and T. Okamoto, *Acc. Chem. Res.*, 2022, **55**, 660–672.
- 67 W. Jiang, Y. Li and Z. Wang, *Acc. Chem. Res.*, 2014, **47**, 3135–3147.
- 68 M. Gsänger, D. Bialas, L. Huang, M. Stolte and F. Würthner, *Adv. Mater.*, 2016, **28**, 3615–3645.
- 69 Z. Liu, Y. Wu, Q. Zhang and X. Gao, *J. Mater. Chem. A*, 2016, **4**, 17604–17622.
- 70 C. Li and H. Wonneberger, *Adv. Mater.*, 2012, **24**, 613–636.
- 71 K. Zhao, Z.-F. Yao, Z.-Y. Wang, J.-C. Zeng, L. Ding, M. Xiong, J.-Y. Wang and J. Pei, *J. Am. Chem. Soc.*, 2022, **144**, 3091–3098.
- 72 V. M. Tsefrikas and L. T. Scott, *Chem. Rev.*, 2006, **106**, 4868–4884.
- 73 Y.-T. Wu and J. S. Siegel, *Chem. Rev.*, 2006, **106**, 4843–4867.
- 74 A. Sygula, F. R. Fronczek, R. Sygula, P. W. Rabideau and M. M. Olmstead, *J. Am. Chem. Soc.*, 2007, **129**, 3842–3843.
- 75 D. Miyajima, K. Tashiro, F. Araoka, H. Takezoe, J. Kim, K. Kato, M. Takata and T. Aida, *J. Am. Chem. Soc.*, 2009, **131**, 44–45.
- 76 D. Pappo, T. Mejuch, O. Reany, E. Solel, M. Gurram and E. Keinan, *Org. Lett.*, 2009, **11**, 1063–1066.
- 77 L. T. Scott, E. A. Jackson, Q. Zhang, B. D. Steinberg, M. Bancu and B. Li, *J. Am. Chem. Soc.*, 2012, **134**, 107–110.
- 78 M. C. Stuparu, *Angew. Chem., Int. Ed.*, 2013, **52**, 7786–7790.
- 79 R.-Q. Lu, Y.-Q. Zheng, Y.-N. Zhou, X.-Y. Yan, T. Lei, K. Shi, Y. Zhou, J. Pei, L. Zoppi, K. K. Baldrige, J. S. Siegel and X.-Y. Cao, *J. Mater. Chem. A*, 2014, **2**, 20515–20519.
- 80 K. Shi, T. Lei, X.-Y. Wang, J.-Y. Wang and J. Pei, *Chem. Sci.*, 2014, **5**, 1041–1045.
- 81 P. L. Abeyratne Kuragama, F. R. Fronczek and A. Sygula, *Org. Lett.*, 2015, **17**, 5292–5295.
- 82 R.-Q. Lu, Y.-N. Zhou, X.-Y. Yan, K. Shi, Y.-Q. Zheng, M. Luo, X.-C. Wang, J. Pei, H. Xia, L. Zoppi, K. K. Baldrige, J. S. Siegel and X.-Y. Cao, *Chem. Commun.*, 2015, **51**, 1681–1684.
- 83 H. Barbero, S. Ferrero, L. Álvarez-Miguel, P. Gómez-Iglesias, D. Miguel and C. M. Álvarez, *Chem. Commun.*, 2016, **52**, 12964–12967.
- 84 A. A. K. Karunathilake, C. M. Thompson, S. Peranathan, J. P. Ferraris and R. A. Smaldone, *Chem. Commun.*, 2016, **52**, 12881–12884.
- 85 X. Li, F. Kang and M. Inagaki, *Small*, 2016, **12**, 3206–3223.
- 86 S. Nakatsuka, N. Yasuda and T. Hatakeyama, *J. Am. Chem. Soc.*, 2018, **140**, 13562–13565.
- 87 S. Kumar and Y.-T. Tao, *Chem. – Asian J.*, 2021, **16**, 621–647.
- 88 Z. Jiang, S. Zhou, W. Jin, C. Zhao, Z. Liu and X. Yu, *Org. Lett.*, 2022, **24**, 1017–1021.
- 89 G. Li, W.-W. Xiong, P.-Y. Gu, J. Cao, J. Zhu, R. Ganguly, Y. Li, A. C. Grimsdale and Q. Zhang, *Org. Lett.*, 2015, **17**, 560–563.

- 90 X.-Y. Wang, F.-D. Zhuang, X.-C. Wang, X.-Y. Cao, J.-Y. Wang and J. Pei, *Chem. Commun.*, 2015, **51**, 4368–4371.
- 91 A. Rademacher, S. Märkle and H. Langhals, *Chem. Ber.*, 1982, **115**, 2927–2934.
- 92 Y. Avlasevich, C. Li and K. Müllen, *J. Mater. Chem.*, 2010, **20**, 3814–3826.
- 93 J. Hoffmann, B. Geffroy, E. Jaques, M. Hissler and A. Staubitz, *J. Mater. Chem. C*, 2021, **9**, 14720–14729.
- 94 E. Clar, C. T. Ironside and M. Zander, *J. Chem. Soc.*, 1959, 142–147, DOI: [10.1039/JR9590000142](https://doi.org/10.1039/JR9590000142).
- 95 A. Stabel, P. Herwig, K. Müllen and J. P. Rabe, *Angew. Chem., Int. Ed. Engl.*, 1995, **34**, 1609–1611.
- 96 L. Schmidt-Mende, A. Fechtenkötter, K. Müllen, E. Moons, R. H. Friend and J. D. MacKenzie, *Science*, 2001, **293**, 1119–1122.
- 97 M. D. Watson, A. Fechtenkötter and K. Müllen, *Chem. Rev.*, 2001, **101**, 1267–1300.
- 98 A. C. Grimsdale and K. Müllen, *Angew. Chem., Int. Ed.*, 2005, **44**, 5592–5629.
- 99 A. C. Grimsdale, J. Wu and K. Müllen, *Chem. Commun.*, 2005, 2197–2204, DOI: [10.1039/B418172G](https://doi.org/10.1039/B418172G).
- 100 J. Wu, W. Pisula and K. Müllen, *Chem. Rev.*, 2007, **107**, 718–747.
- 101 K. Müllen and J. P. Rabe, *Acc. Chem. Res.*, 2008, **41**, 511–520.
- 102 L. Chen, Y. Hernandez, X. Feng and K. Müllen, *Angew. Chem., Int. Ed.*, 2012, **51**, 7640–7654.
- 103 H. Seyler, B. Purushothaman, D. J. Jones, A. B. Holmes and W. W. H. Wong, *Pure Appl. Chem.*, 2012, **84**, 1047–1067.
- 104 M. Krieg, F. Reicherter, P. Haiss, M. Ströbele, K. Eichele, M.-J. Treanor, R. Schaub and H. F. Bettinger, *Angew. Chem., Int. Ed.*, 2015, **54**, 8284–8286.
- 105 J. Dosso, J. Tasseroul, F. Fasano, D. Marinelli, N. Biot, A. Fermi and D. Bonifazi, *Angew. Chem., Int. Ed.*, 2017, **56**, 4483–4487.
- 106 P. B. Pati, E. Jin, Y. Kim, Y. Kim, J. Mun, S. J. Kim, S. J. Kang, W. Choe, G. Lee, H.-J. Shin and Y. S. Park, *Angew. Chem., Int. Ed.*, 2020, **59**, 14891–14895.
- 107 T. Sakamaki, T. Nakamuro, K. Yamashita, K. Hirata, R. Shang and E. Nakamura, *Chem. Mater.*, 2021, **33**, 5337–5344.
- 108 J. Roncali, *Chem. Rev.*, 1997, **97**, 173–206.
- 109 M. Bendikov, F. Wudl and D. F. Perepichka, *Chem. Rev.*, 2004, **104**, 4891–4946.
- 110 P. Prins, F. C. Grozema, J. M. Schins, S. Patil, U. Scherf and L. D. A. Siebbeles, *Phys. Rev. Lett.*, 2006, **96**, 146601.
- 111 K. Takimiya, S. Shinamura, I. Osaka and E. Miyazaki, *Adv. Mater.*, 2011, **23**, 4347–4370.
- 112 H. Tsuji and E. Nakamura, *Acc. Chem. Res.*, 2017, **50**, 396–406.
- 113 Z. Cai, M. A. Awais, N. Zhang and L. Yu, *Chem*, 2018, **4**, 2538–2570.
- 114 J. Chen, K. Yang, X. Zhou and X. Guo, *Chem. – Asian J.*, 2018, **13**, 2587–2600.
- 115 H. Hopf, *Angew. Chem., Int. Ed.*, 2013, **52**, 12224–12226.
- 116 M. Saito, *Symmetry*, 2010, **2**, 950–969.
- 117 C. Ma, J. Zhang, J. Li and C. Cui, *Chem. Commun.*, 2015, **51**, 5732–5734.
- 118 M. M. Morgan, E. A. Patrick, J. M. Rautiainen, H. M. Tuononen, W. E. Piers and D. M. Spasyuk, *Organometallics*, 2017, **36**, 2541–2551.
- 119 F.-D. Zhuang, Z.-H. Sun, Z.-F. Yao, Q.-R. Chen, Z. Huang, J.-H. Yang, J.-Y. Wang and J. Pei, *Angew. Chem., Int. Ed.*, 2019, **58**, 10708–10712.
- 120 O. V. Serdyuk, A. V. Gulevskaya, A. F. Pozharskii and V. E. Avakyan, *J. Heterocycl. Chem.*, 2008, **45**, 195–199.
- 121 A. V. Gulevskaya, O. V. Serduke, A. F. Pozharskii and D. V. Besedin, *Tetrahedron*, 2003, **59**, 7669–7679.
- 122 D. J. H. Emslie, W. E. Piers and M. Parvez, *Angew. Chem., Int. Ed.*, 2003, **42**, 1252–1255.
- 123 C. A. Jaska, D. J. H. Emslie, M. J. D. Bosdet, W. E. Piers, T. S. Sorensen and M. Parvez, *J. Am. Chem. Soc.*, 2006, **128**, 10885–10896.
- 124 C. A. Jaska, W. E. Piers, R. McDonald and M. Parvez, *J. Org. Lett.*, 2007, **72**, 5234–5243.
- 125 B. Neue, J. F. Araneda, W. E. Piers and M. Parvez, *Angew. Chem., Int. Ed.*, 2013, **52**, 9966–9969.
- 126 M. J. D. B. J. D. Bosdet, W. E. P. E. Piers, T. S. S. S. Sorensen and M. Parvez, *Can. J. Chem.*, 2010, **88**, 426–433.
- 127 X. Wang, F. Zhang, J. Liu, R. Tang, Y. Fu, D. Wu, Q. Xu, X. Zhuang, G. He and X. Feng, *Org. Lett.*, 2013, **15**, 5714–5717.
- 128 X. Wang, F. Zhang, J. Gao, Y. Fu, W. Zhao, R. Tang, W. Zhang, X. Zhuang and X. Feng, *J. Org. Lett.*, 2015, **80**, 10127–10133.
- 129 W. Zhang, F. Zhang, R. Tang, Y. Fu, X. Wang, X. Zhuang, G. He and X. Feng, *Org. Lett.*, 2016, **18**, 3618–3621.
- 130 Y. Han, W. Yuan, H. Wang, M. Li, W. Zhang and Y. Chen, *J. Mater. Chem. C*, 2018, **6**, 10456–10463.
- 131 J. Zhang, F. Liu, Z. Sun, C. Li, Q. Zhang, C. Zhang, Z. Liu and X. Liu, *Chem. Commun.*, 2018, **54**, 8178–8181.
- 132 M. Tasior and D. T. Gryko, *J. Org. Lett.*, 2016, **81**, 6580–6586.
- 133 M. Lepeltier, O. Lukyanova, A. Jacobson, S. Jeeva and D. F. Perepichka, *Chem. Commun.*, 2010, **46**, 7007–7009.
- 134 C.-J. Sun, N. Wang, T. Peng, X. Yin, S. Wang and P. Chen, *Inorg. Chem.*, 2019, **58**, 3591–3595.
- 135 T. Hatakeyama, S. Hashimoto, S. Seki and M. Nakamura, *J. Am. Chem. Soc.*, 2011, **133**, 18614–18617.
- 136 D. Tian, Q. Li, Y. Zhao, Z. Wang, W. Li, S. Xia, S. Xing, B. Zhu, J. Zhang and C. Cui, *J. Org. Lett.*, 2020, **85**, 526–536.
- 137 H. Xin, J. Li, X. Yang and X. Gao, *J. Org. Lett.*, 2020, **85**, 70–78.
- 138 D.-T. Yang, T. Nakamura, Z. He, X. Wang, A. Wakamiya, T. Peng and S. Wang, *Org. Lett.*, 2018, **20**, 6741–6745.
- 139 P. Qiang, Z. Sun, M. Wan, X. Wang, P. Thiruvengadam, C. Bingi, W. Wei, W. Zhu, D. Wu and F. Zhang, *Org. Lett.*, 2019, **21**, 4575–4579.
- 140 Y. Fu, K. Zhang, E. Dmitrieva, F. Liu, J. Ma, J. J. Weigand, A. A. Popov, R. Berger, W. Pisula, J. Liu and X. Feng, *Org. Lett.*, 2019, **21**, 1354–1358.
- 141 M. Numano, N. Nagami, S. Nakatsuka, T. Katayama, K. Nakajima, S. Tatsumi, N. Yasuda and T. Hatakeyama, *Chem. – Eur. J.*, 2016, **22**, 11574–11577.



- 142 G. H. M. Davies and G. A. Molander, *J. Org. Lett.*, 2016, **81**, 3771–3779.
- 143 G. H. M. Davies, A. Mukhtar, B. Saeednia, F. Sherafat, C. B. Kelly and G. A. Molander, *J. Org. Lett.*, 2017, **82**, 5380–5390.
- 144 M. Fingerle and H. F. Bettinger, *Chem. Commun.*, 2020, **56**, 3847–3850.
- 145 Z. Sun, C. Yi, Q. Liang, C. Bingi, W. Zhu, P. Qiang, D. Wu and F. Zhang, *Org. Lett.*, 2020, **22**, 209–213.
- 146 X. Wang, F. Zhang, K. S. Schellhammer, P. Machata, F. Ortmann, G. Cuniberti, Y. Fu, J. Hunger, R. Tang, A. A. Popov, R. Berger, K. Müllen and X. Feng, *J. Am. Chem. Soc.*, 2016, **138**, 11606–11615.
- 147 M. R. Ajayakumar, Y. Fu, J. Ma, F. Hennersdorf, H. Komber, J. J. Weigand, A. Alfonsov, A. A. Popov, R. Berger, J. Liu, K. Müllen and X. Feng, *J. Am. Chem. Soc.*, 2018, **140**, 6240–6244.
- 148 M. R. Ajayakumar, Y. Fu, F. Liu, H. Komber, V. Tkachova, C. Xu, S. Zhou, A. A. Popov, J. Liu and X. Feng, *Chem. – Eur. J.*, 2020, **26**, 7497–7503.
- 149 Y. Fu, X. Chang, H. Yang, E. Dmitrieva, Y. Gao, J. Ma, L. Huang, J. Liu, H. Lu, Z. Cheng, S. Du, H.-J. Gao and X. Feng, *Angew. Chem., Int. Ed.*, 2021, **60**, 26115–26121.
- 150 M. Zhao and Q. Miao, *Angew. Chem., Int. Ed.*, 2021, **60**, 21289–21294.
- 151 S. Pios, X. Huang, A. L. Sobolewski and W. Domcke, *Phys. Chem. Chem. Phys.*, 2021, **23**, 12968–12975.
- 152 C.-W. Ju, B. Li, L. Li, W. Yan, C. Cui, X. Ma and D. Zhao, *J. Am. Chem. Soc.*, 2021, **143**, 5903–5916.
- 153 H. Helten, *Chem. – Eur. J.*, 2016, **22**, 12972–12982.
- 154 A. W. Baggett, F. Guo, B. Li, S.-Y. Liu and F. Jäkle, *Angew. Chem., Int. Ed.*, 2015, **54**, 11191–11195.
- 155 Y. Chen, W. Chen, Y. Qiao, X. Lu and G. Zhou, *Angew. Chem., Int. Ed.*, 2020, **59**, 7122–7130.
- 156 K. Boknevit, C. Darrigan, A. Chrostowska and S.-Y. Liu, *Chem. Commun.*, 2020, **56**, 3749–3752.
- 157 S. Tsuchiya, H. Saito, K. Nogi and H. Yorimitsu, *Org. Lett.*, 2019, **21**, 3855–3860.
- 158 I. Shin, H. N. Lim and W. P. Hong, *Synthesis*, 2022, 570–588.
- 159 A. Abengózar, P. García-García, M. A. Fernández-Rodríguez, D. Sucunza and J. J. Vaquero, *Adv. Heterocycl. Chem.*, 2021, **135**, 197–259.
- 160 Z. X. Giustra and S.-Y. Liu, *J. Am. Chem. Soc.*, 2018, **140**, 1184–1194.
- 161 K. Mitsudo, K. Shigemori, H. Mandai, A. Wakamiya and S. Suga, *Org. Lett.*, 2018, **20**, 7336–7340.
- 162 C. Bronner, S. Stremlau, M. Gille, F. Brauße, A. Haase, S. Hecht and P. Tegeder, *Angew. Chem., Int. Ed.*, 2013, **52**, 4422–4425.
- 163 J. Cai, C. A. Pignedoli, L. Talirz, P. Ruffieux, H. Söde, L. Liang, V. Meunier, R. Berger, R. Li, X. Feng, K. Müllen and R. Fasel, *Nat. Nanotechnol.*, 2014, **9**, 896–900.
- 164 S. Kawai, S. Saito, S. Osumi, S. Yamaguchi, A. S. Foster, P. Spijker and E. Meyer, *Nat. Commun.*, 2015, **6**, 8098.
- 165 R. R. Cloke, T. Marangoni, G. D. Nguyen, T. Joshi, D. J. Rizzo, C. Bronner, T. Cao, S. G. Louie, M. F. Crommie and F. R. Fischer, *J. Am. Chem. Soc.*, 2015, **137**, 8872–8875.
- 166 S. Kawai, S. Nakatsuka, T. Hatakeyama, R. Pawlak, T. Meier, J. Tracey, E. Meyer and S. Foster Adam, *Sci. Adv.*, 2018, **4**, 7181.
- 167 J.-J. Zhang, L. Yang, F. Liu, Y. Fu, J. Liu, A. A. Popov, J. Ma and X. Feng, *Angew. Chem., Int. Ed.*, 2021, **60**, 25695–25700.
- 168 Y. Kondo, K. Yoshiura, S. Kitera, H. Nishi, S. Oda, H. Gotoh, Y. Sasada, M. Yanai and T. Hatakeyama, *Nat. Photon.*, 2019, **13**, 678–682.
- 169 H. Tanaka, S. Oda, G. Ricci, H. Gotoh, K. Tabata, R. Kawasumi, D. Beljonne, Y. Olivier and T. Hatakeyama, *Angew. Chem., Int. Ed.*, 2021, **60**, 17910–17914.
- 170 S. Oda, B. Kawakami, Y. Yamasaki, R. Matsumoto, M. Yoshioka, D. Fukushima, S. Nakatsuka and T. Hatakeyama, *J. Am. Chem. Soc.*, 2022, **144**, 106–112.
- 171 K. Matsui, S. Oda, K. Yoshiura, K. Nakajima, N. Yasuda and T. Hatakeyama, *J. Am. Chem. Soc.*, 2018, **140**, 1195–1198.
- 172 S. Oda, B. Kawakami, R. Kawasumi, R. Okita and T. Hatakeyama, *Org. Lett.*, 2019, **21**, 9311–9314.
- 173 J. A. Knöller, G. Meng, X. Wang, D. Hall, A. Pershin, D. Beljonne, Y. Olivier, S. Laschat, E. Zysman-Colman and S. Wang, *Angew. Chem., Int. Ed.*, 2020, **59**, 3156–3160.
- 174 N. Ikeda, S. Oda, R. Matsumoto, M. Yoshioka, D. Fukushima, K. Yoshiura, N. Yasuda and T. Hatakeyama, *Adv. Mater.*, 2020, **32**, 2004072.
- 175 M. Nagata, H. Min, E. Watanabe, H. Fukumoto, Y. Mizuhata, N. Tokitoh, T. Agou and T. Yasuda, *Angew. Chem., Int. Ed.*, 2021, **60**, 20280–20285.
- 176 S. M. Suresh, E. Duda, D. Hall, Z. Yao, S. Bagnich, A. M. Z. Slawin, H. Bässler, D. Beljonne, M. Buck, Y. Olivier, A. Köhler and E. Zysman-Colman, *J. Am. Chem. Soc.*, 2020, **142**, 6588–6599.
- 177 X. Liang, Z.-P. Yan, H.-B. Han, Z.-G. Wu, Y.-X. Zheng, H. Meng, J.-L. Zuo and W. Huang, *Angew. Chem., Int. Ed.*, 2018, **57**, 11316–11320.
- 178 Y. Zhang, D. Zhang, J. Wei, Z. Liu, Y. Lu and L. Duan, *Angew. Chem., Int. Ed.*, 2019, **58**, 16912–16917.
- 179 M. Yang, I. S. Park and T. Yasuda, *J. Am. Chem. Soc.*, 2020, **142**, 19468–19472.
- 180 J.-K. Li, X.-Y. Chen, Y.-L. Guo, X.-C. Wang, A. C. H. Sue, X.-Y. Cao and X.-Y. Wang, *J. Am. Chem. Soc.*, 2021, **143**, 17958–17963.
- 181 Y. Zhang, D. Zhang, T. Huang, A. J. Gillett, Y. Liu, D. Hu, L. Cui, Z. Bin, G. Li, J. Wei and L. Duan, *Angew. Chem., Int. Ed.*, 2021, **60**, 20498–20503.
- 182 Y. Xu, Z. Cheng, Z. Li, B. Liang, J. Wang, J. Wei, Z. Zhang and Y. Wang, *Adv. Opt. Mater.*, 2020, **8**, 1902142.
- 183 S. Oda, W. Kumano, T. Hama, R. Kawasumi, K. Yoshiura and T. Hatakeyama, *Angew. Chem., Int. Ed.*, 2021, **60**, 2882–2886.
- 184 J. V. Caspar and T. J. Meyer, *J. Phys. Chem.*, 1983, **87**, 952–957.
- 185 J. V. Caspar, E. M. Kober, B. P. Sullivan and T. J. Meyer, *J. Am. Chem. Soc.*, 1982, **104**, 630–632.

- 186 N. Boens, B. Verbelen, M. J. Ortiz, L. Jiao and W. Dehaen, *Coordin. Chem. Rev.*, 2019, **399**, 213024.
- 187 W. Sun, X. Zhao, J. Fan, J. Du and X. Peng, *Small*, 2019, **15**, 1804927.
- 188 Z. Shi, X. Han, W. Hu, H. Bai, B. Peng, L. Ji, Q. Fan, L. Li and W. Huang, *Chem. Soc. Rev.*, 2020, **49**, 7533–7567.
- 189 D. Li, H. Zhang and Y. Wang, *Chem. Soc. Rev.*, 2013, **42**, 8416–8433.
- 190 C. Dou, J. Liu and L. Wang, *Sci. China: Chem.*, 2017, **60**, 450–459.
- 191 R. Zhao, J. Liu and L. Wang, *Acc. Chem. Res.*, 2020, **53**, 1557–1567.
- 192 J. Miao, Y. Wang, J. Liu and L. Wang, *Chem. Soc. Rev.*, 2022, **51**, 153–187.
- 193 A. Wakamiya, T. Taniguchi and S. Yamaguchi, *Angew. Chem., Int. Ed.*, 2006, **45**, 3170–3173.
- 194 S. K. Murphy, C. Baik, J.-S. Lu and S. Wang, *Org. Lett.*, 2010, **12**, 5266–5269.
- 195 C. Baik, S. K. Murphy and S. Wang, *Angew. Chem., Int. Ed.*, 2010, **49**, 8224–8227.
- 196 C. Zhu, Z.-H. Guo, A. U. Mu, Y. Liu, S. E. Wheeler and L. Fang, *J. Org. Lett.*, 2016, **81**, 4347–4352.
- 197 M. M. Morgan, M. Nazari, T. Pickl, J. M. Rautiainen, H. M. Tuononen, W. E. Piers, G. C. Welch and B. S. Gelfand, *Chem. Commun.*, 2019, **55**, 11095–11098.
- 198 M. Tasiar, P. Kowalczyk, M. Przybył, M. Czichy, P. Janasik, M. H. E. Bousquet, M. Łapkowski, M. Rammo, A. Rebane, D. Jacquemin and D. T. Gryko, *Chem. Sci.*, 2021, **12**, 15935–15946.
- 199 X. Zhu, C. Mitsui, H. Tsuji and E. Nakamura, *J. Am. Chem. Soc.*, 2009, **131**, 13596–13597.
- 200 X. Zhu, H. Tsuji, J. T. López Navarrete, J. Casado and E. Nakamura, *J. Am. Chem. Soc.*, 2012, **134**, 19254–19259.
- 201 H. Tsuji and E. Nakamura, *Acc. Chem. Res.*, 2019, **52**, 2939–2949.
- 202 H. Lu, T. Nakamuro, K. Yamashita, H. Yanagisawa, O. Nureki, M. Kikkawa, H. Gao, J. Tian, R. Shang and E. Nakamura, *J. Am. Chem. Soc.*, 2020, **142**, 18990–18996.
- 203 Y. Yang, R. C. da Costa, M. J. Fuchter and A. J. Campbell, *Nat. Photon.*, 2013, **7**, 634–638.
- 204 L. Zhang, I. Song, J. Ahn, M. Han, M. Linares, M. Surin, H.-J. Zhang, J. H. Oh and J. Lin, *Nat. Commun.*, 2021, **12**, 142.
- 205 M. Sapir and E. V. Donckt, *Chem. Phys. Lett.*, 1975, **36**, 108–110.
- 206 N. I. Nijegorodov and W. S. Downey, *J. Phys. Chem.*, 1994, **98**, 5639–5643.
- 207 J. Full, S. P. Panchal, J. Götz, A.-M. Krause and A. Nowak-Król, *Angew. Chem., Int. Ed.*, 2021, **60**, 4350–4357.
- 208 L. Jiang, Y. Wang, D. Tan, X. Chen, T. Ma, B. Zhang and D.-T. Yang, *Chem. Sci.*, 2022, **13**, 5597–5605.
- 209 G. Meng, L. Liu, Z. He, D. Hall, X. Wang, T. Peng, X. Yin, P. Chen, D. Beljonne, Y. Olivier, E. Zysman-Colman, N. Wang and S. Wang, *Chem. Sci.*, 2022, **13**, 1665–1674.
- 210 C. Zhu, X. Ji, D. You, T. L. Chen, A. U. Mu, K. P. Barker, L. M. Klivansky, Y. Liu and L. Fang, *J. Am. Chem. Soc.*, 2018, **140**, 18173–18182.
- 211 Y. Cao, C. Zhu, M. Barlóg, K. P. Barker, X. Ji, A. J. Kalin, M. Al-Hashimi and L. Fang, *J. Org. Lett.*, 2021, **86**, 2100–2106.
- 212 F. Liu, Z. Ding, J. Liu and L. Wang, *Chem. Commun.*, 2017, **53**, 12213–12216.
- 213 F. Qiu, F. Zhang, R. Tang, Y. Fu, X. Wang, S. Han, X. Zhuang and X. Feng, *Org. Lett.*, 2016, **18**, 1398–1401.
- 214 K. Liu, R. A. Lalancette and F. Jäkle, *J. Am. Chem. Soc.*, 2017, **139**, 18170–18173.
- 215 K. Liu, R. A. Lalancette and F. Jäkle, *J. Am. Chem. Soc.*, 2019, **141**, 7453–7462.
- 216 J.-J. Zhang, J. Ma, F. Liu, L.-S. Cui, Y. Fu, L. Yang, A. A. Popov, J. J. Weigand, J. Liu and X. Feng, *Org. Lett.*, 2022, **24**, 1877–1882.